From Structure-Activity Relationships on Thiazole Derivatives to the *In Vivo* Evaluation of a New Radiotracer for Cannabinoid Subtype 2 PET Imaging

Fabien Caillé[†,1], Fanny Cacheux[†,1], Marie-Anne Peyronneau,[1] Benoît Jego,[1] Emilie Jaumain,[1] Géraldine Pottier,[1] Christoph Ullmer,[2] Uwe Grether,[2] Alexandra Winkeler,[1] Frédéric Dollé,[1] Annelaure Damont[1] and Bertrand Kuhnast[*,1]

[1]UMR 1023 IMIV, Service Hospitalier Frédéric Joliot, CEA, Inserm, Université Paris Sud, CNRS, Université Paris-Saclay, Orsay, France

[2]Roche Innovation Center Basel, F. Hoffmann-La Roche Ltd., Basel, Switzerland

[*]corresponding author: bertrand.kuhnast@cea.fr

ORCID iD Bertrand Kuhnast : 0000-0002-5035-4072

[†] these authors contributed equally to this work

Abstract: Upregulation of the cannabinoid type 2 receptors (CB_2R) unveils inflammation processes of pathological disorders such as cancer, pain or neurodegenerative diseases. Among others, CB_2R agonist A-836339 has been labeled with carbon-11 for PET imaging of the CB_2R and displayed promising results in a mouse model of Alzheimer's disease. The aim of the present work was to develop fluorinated analogs of A-836339 for labeling with fluorine-18 to design a new PET tracer for CB_2R imaging. Seven fluorinated analogs of A-836339 were synthesized in two to three steps and their binding affinities and selectivities for both the human and the mouse CB_2R were measured as well as their early ADME profiles. Among them, compound **2f** (K_{ihCB2R} = 0.1 nM, K_{ihCB1R}/ K_{ihCB2R} = 300) displayed high affinity and selectivity for CB_2R but also promising lipophilicity, kinetic solubility and membrane permeation properties and was further selected for *in vitro* metabolism studies. Incubation of **2f** with human or rat liver microsomes followed by LC/MS analysis revealed the presence of six different metabolites mainly resulting from oxidation reactions. A tosylated precursor of **2f** was synthesized in two steps and radiolabeled with fluorine-18 to afford [^{18}F]**2f** in 15 ± 5% radiochemical yield and a molar activity of 110 ± 30 GBq/μmol. Autoradiographies of rat spleen and biodistribution studies in healthy rats including pre-treatments with either CB_2R or CB_1R-specific compounds suggested that [^{18}F]**2f** is a specific tracer for the CB_2R *in vivo*. We have therefore demonstrated here that [^{18}F]**2f** is a promising novel tracer for imaging CB_2R *in vivo* using PET. Further investigation in animal models of inflammation will follow.

Keywords: cannabinoid type 2, PET imaging, fluorine-18

INTRODUCTION

The endocannabinoid system plays a homeostatic role in various physiological and pathological conditions and represents a potent therapeutic target for which a large variety of drugs has been tested over the past decade.[1] It is essentially constituted of two G-protein coupled receptors, namely the cannabinoid subtype 1 receptors (CB$_1$R) highly expressed in the central nervous system[2] and the cannabinoid subtype 2 receptors (CB$_2$R) predominant at the periphery on immune cells.[3] Indeed, CB$_2$R have been observed on macrophages at the marginal zone of the spleen[4] but also in tonsils, on B-cells, T-cells and natural killer cells.[3] More recently, CB$_2$R have been found at low concentration in the brain on microglial cells,[5,6] human fetal astrocytes[7] and cerebromicrovascular endothelial cells.[8]

CB$_2$R play an important role in immunoregulation through the inhibition of the adenyl cyclase activity, the activation of the p42/p44 MAP kinase and the modulation of Ca^{2+} ion channels.[9] CB$_2$R activation is immunomodulatory and neuroprotective and CB$_2$R agonists proved to reduce both acute and neuropathic pain, making this receptor an interesting therapeutic target.[10] Numerous agonists of the CB$_2$R with a large variety of physico-chemical properties have been developed, some presenting high selectivity to activate distinct signaling pathways and decrease off-target side effects. [11]

CB$_2$R are also an appealing target to track inflammation processes as their expression level increases in tissues upon pathological stimuli. Overexpression of CB$_2$R has been reported in various inflammation-related disorders including cancer,[12] pain, atherosclerosis and liver diseases.[13] Moreover, up-regulation of CB$_2$R upon microglia activation unveils neuroinflammatory processes associated with neurodegenerative diseases such as Alzheimer's disease (AD),[14] multiple and amyotrophic lateral sclerosis,[15] Parkinson's[16] or Huntington's disease.[17] Molecular imaging using positron emission tomography (PET) is a state-of-the-art technique to diagnose non-invasively numerous pathologies and monitor disease progression for therapeutic purposes. Moreover, the high sensitivity of PET imaging associated with mathematical models of quantification of the radioactive signal is a powerful combination to explore central nervous system receptors present even at very low concentrations. Considering the strong potential of the CB$_2$R, several PET tracers have been developed to explore these receptors under pathological conditions (Figure 1).[18] GW405833, a CB$_2$R partial agonist known to cross the blood brain barrier has been labeled with carbon-11 (t$_{1/2}$ = 20.4 min) and showed specific and reversible binding to the rat striatum after stereotactic injection of viral vectors encoding the human CB$_2$ receptor gene.[19] A first-in-man study has been conducted with [^{11}C]NE40 for biodistribution and dosimetry studies on healthy subjects.[20] More recently, inflamed carotid plaques in a mouse model of atherosclerosis were identified by PET imaging using the CB$_2$R-specific carbon-11 radiotracer [^{11}C]RS-016.[21]
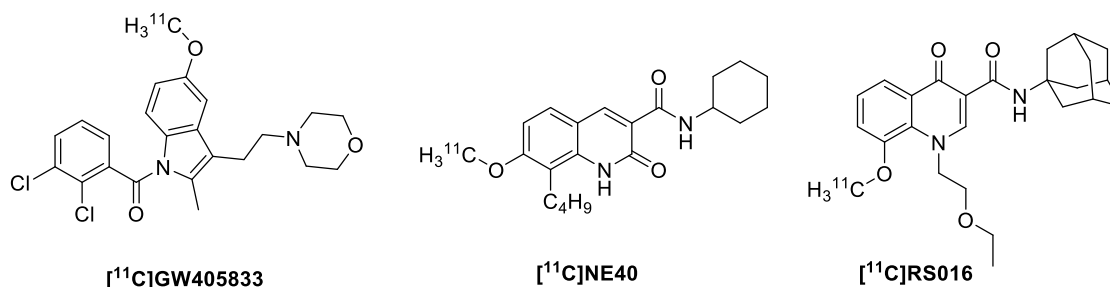
Figure 1. Structure of three carbon-11-labeled radiotracers for CB$_2$R imaging.

Among the variety of radiotracers developed for CB$_2$R PET imaging, A-836339 [2,2,3,3-tetramethylcyclopropanecarboxylic acid [3-(2-methoxy-ethyl)-4,5-dimethyl-3H-thiazol-(2Z)-ylidene]amide] (**1**, Figure 2) is a selective agonist with high binding affinity for human CB$_2$R (K$_i$ = 0.64 nM)[22] which has been labeled with carbon-11 and exhibits high specific cerebral uptake in a mouse model of AD.[23] Furthermore, a complementary study on a mouse model of Aβ-amyloidosis showed that [^{11}C]A-836339 is a potent specific radiotracer for neuroinflammation in early preclinical stages of AD.[24] However, [^{11}C]A-836339 showed disappointing results when monitoring low CB$_2$R expression in LPS, AMPA and cerebral ischemia rat models of neuroinflammation.[25]

Very recently, Moldovan and coworkers developed a series of fluorinated derivatives of A-836339 with high affinity for CB$_2$R (K$_i$ down to 0.31 nM) and good selectivity towards CB$_1$R (K$_i$ up to 1600 nM for CB$_1$R).[26] From their structure-activity relationship study emerged compound **2c** (Figure 2) which was labeled with fluorine-18 (t$_{1/2}$ = 109.8 min). Small animal PET studies with the resulting radiotracer shows promising results in a LPS mouse model of neuroinflammation but very rapid metabolization limits further investigations.

In parallel to the work conducted by Moldovan *et al.*, we have developed a similar series of seven fluorinated analogs of A-836339 (Figure 2). Those compounds have been tested for their affinity with human and mouse CB$_2$R and their selectivity towards human CB$_1$R together with their functional activity and selectivity for those receptors. Early absorption, distribution, metabolism and excretion (ADME) profiles were also determined and, among other criteria, the microsomal and hepatocyte clearances of the compounds led us to choose a different derivative for fluorine-18 labeling, namely compound **2f**, which displays one of the highest affinity and selectivity for CB$_2$R among this series of compounds. Since metabolism is a key question to assess for a potential PET tracer, compound **2f** was incubated with either human or rat liver microsomes and LC/MS and MS^n analysis were performed on the extracts to determine the metabolic pathways. *In vivo*, the metabolic stability of [^{18}F]**2f** was measured in plasma. A tosylated precursor was synthesized to afford [^{18}F]**2f** after automated fluorine-18 radiolabeling. *Ex vivo* biodistribution in rats including pre-saturation with either a selective CB$_2$R agonist or a selective CB$_1$R agonist and autoradiographies of rat spleens were realized to assess the potential of [^{18}F]**2f** to bind CB$_2$R *in vivo*.

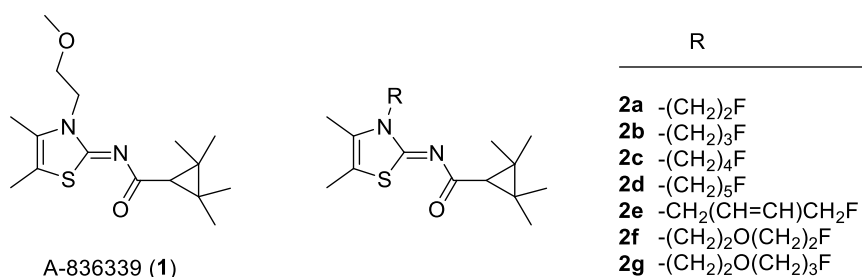|	R
2a	-(CH$_2$)$_2$F
2b	-(CH$_2$)$_3$F
2c	-(CH$_2$)$_4$F
2d	-(CH$_2$)$_5$F
2e	-CH$_2$(CH=CH)CH$_2$F
2f	-(CH$_2$)$_2$O(CH$_2$)$_2$F
2g	-(CH$_2$)$_2$O(CH$_2$)$_3$F

A-836339 (**1**)

Figure 2. Structures of compound A-836339 and fluorinated analogs **2a-2g**.

EXPERIMENTAL SECTION

Chemistry

Chemicals were purchased from Aldrich (France) and used as received. Flash chromatographies were conducted on silica gel (0.63-0.200 mm, VWR, France) columns. Reactions were monitored by thin layer chromatography (TLC) on aluminum pre-coated plates of silica gel 60F$_{254}$ (VWR, France). The compounds were localized at 254 nm using a UV-lamp or using a KMnO$_4$ stain solution. ^{1}H and ^{13}C NMR spectra were recorded on a Bruker Advance 400 MHz apparatus using CDCl$_3$ or DMF-d_7 as solvents. The chemical shifts (δ) are reported in ppm, downfield from TMS (s, d, t, q, m and b for singlet, doublet, triplet, quadruplet, multiplet and broad respectively) and referenced with the solvent residual chemical shift. High resolution mass spectrometry analyses (HRMS) were performed by the Small Molecule Mass Spectrometry platform of IMAGIF, (Gif-sur-Yvette, France, www.imagif.cnrs.fr) by electrospray with positive (ESI+) or negative (ESI-) ionization mode. Melting points (M. p.) were measured with an Electrothermal IA9200 and are reported in °C.

(Z)-N-(3-(2-methoxyethyl)-4,5-dimethylthiazol-2(3H)-ylidene)-2,2,3,3-tetramethylcyclopropane-1-carboxamide (A-836339, 1). Reference compound A-836339 (**1**) was synthesized according to the procedure described by Horti *et al.*.[23] Analytical data (^{1}H-NMR and ^{13}C-NMR) were in accordance with those originally reported.

General procedure for the preparation of compounds 2a-f, 3 and 4: 4,5-dimethylthiazol-2-amine (1.0 equiv.) and the appropriate fluorinated alkyl agent (1.3 equiv.) were stirred neat at 85 °C overnight. Upon cooling to room temperature, the mixture was diluted with dichloromethane (10 mL) and triethylamine (3.0 equiv.), 2,2,3,3-tetramethylcyclopropane-1-carboxylic acid (1.0 equiv.) and BOP (1.4 equiv.) were successively added. The reaction mixture was stirred at room temperature for 12 h. Water (5 mL) was added and the organic layer separated. The aqueous layer was extracted with dichloromethane (3 x 100 mL). The combined organic layers were washed with an aqueous hydrochloric acid (0.1 M, 10 mL), aqueous sodium bicarbonate (1 M, 10 mL), brine (15 mL), dried over sodium sulfate, filtered and concentrated to dryness under vacuum. The residue was purified by flash chromatography on silica gel (using a mixture of ethyl acetate and heptane, or pure dichloromethane) to afford the desired products **2a-f**, **3** and **4**.

(Z)-*N*-(3-(2-fluoroethyl)-4,5-dimethylthiazol-2(3H)-ylidene)-2,2,3,3-tetramethylcyclopropane-1-carboxamide (2a). This derivative was prepared using 200 mg of 4,5-dimethylthiazol-2-amine (1.56 mmol) and 443 mg of 2-fluoroethyl 4-methylbenzenesulfonate (2.03 mmol). Purification by flash chromatography (heptane / ethyl acetate 8/2 v/v) afforded **2a** (68 mg, 15 %) as a white solid. R_f (heptane / ethyl acetate 7/3 v/v): 0.62. M.p.: 123.1 – 124.6 °C. ^{1}H-NMR (CDCl$_3$, 400 MHz) δ 4.74 (dt, 2H, J = 4.8 Hz, J^1_{H-F} = 48.0 Hz), 4.34 (dt, 2H, J = 4.8 Hz, J^2_{H-F} = 24 Hz), 2.16 (s, 3H), 2.14 (s, 3H), 1.49 (s, 1H), 1.31 (s, 6H), 1.18 (s, 6H) ppm. ^{13}C-NMR (CDCl$_3$, 100 MHz) δ 181.3 [C], 164.3 [C], 127.8 [C], 112.8 [C], 81.4 [CH$_2$, d, J^1_{C-F} = 168 Hz], 46.4 [CH$_2$, d, J^2_{C-F} = 20 Hz], 42.2 [CH], 30.3 [2C], 23.9 [2CH$_3$], 16.9 [2CH$_3$], 11.5 [CH$_3$], 11.2 [CH$_3$] ppm. HR-ESI(+)-MS m/z calcd for C$_{13}$H$_{21}$ClN$_3$O$_2$: 286.1244 [M+H]$^+$, found 286.1248.

(Z)-*N*-(3-(3-fluoropropyl)-4,5-dimethylthiazol-2(3H)-ylidene)-2,2,3,3-tetramethylcyclopropane-1-carboxamide (2b). This derivative was prepared using 200 mg of 4,5-dimethylthiazol-2-amine (1.56 mmol) and 471 mg of 2-fluoropropyl 4-methylbenzenesulfonate (2.03 mmol). Purification by flash chromatography (heptane / ethyl acetate 8/2 v/v) afforded **2b** (134 mg, 27 %) as a white solid. R_f (heptane / ethyl acetate 2/1 v/v): 0.39. M.p.: 123.8 – 128.8 °C. ^{1}H-NMR (DMF-d_7, 400 MHz) δ 4.73 (dt, 2H, J = 5.6 Hz, J^1_{H-F} = 47.2 Hz),4.43 (t, 2H, J = 7.2 Hz), 2.99 (db, J^2_{H-F} = 68 Hz), 2.36 (s, 3H), 2.30 (s, 3H), 1.67 (s, 1H), 1.45 (s, 6H), 1.36 (s, 6H) ppm. ^{13}C-NMR (DMF-d_7, 100 MHz) δ 180.2 [C], 164.1 [C], 128.6 [C], 112.7 [C], 81.9 [CH$_2$, d, J^1_{C-F} = 162 Hz], 42.9 [CH$_2$, d, J^3_{C-F} = 6 Hz], 42.1 [CH], 30.3 [2C], 29.4 [CH$_2$], d, J^2_{C-F} = 19 Hz], 23.6 [2CH$_3$], 16.6 [2CH$_3$], 10.9 [CH$_3$], 10.3 [CH$_3$] ppm. HR-ESI(+)-MS m/z calcd for C$_{16}$H$_{25}$FN$_2$OS: 313.1744 [M+H]$^+$, found 313.1738.

(Z)-*N*-(3-(4-fluorobutyl)-4,5-dimethylthiazol-2(3H)-ylidene)-2,2,3,3-tetramethylcyclopropane-1-carboxamide (2c). This derivative was prepared using 200 mg of 4,5-dimethylthiazol-2-amine (1.56 mmol) and 0.21 mL of 4-bromo-1-fluorobutane (2.03 mmol). Purification by flash chromatography (heptane / ethyl acetate 8/2 v/v) afforded **2c** (115 mg, 22 %) as a white solid. R_f (heptane / ethyl acetate 2/1 v/v): 0.41. M.p.: 107.2 – 109.5 °C. ^{1}H-NMR (CDCl$_3$, 400 MHz) δ 4.51 (dt, 2H, J = 5.6 Hz, J^1_{H-F} = 48.0 Hz), 4.14 (t, 2H, J = 5.6 Hz), 2.17 (s, 3H), 2.14 (s, 3H), 1.87-1.72 (m, 4H), 1.51 (s, 1H), 1.33 (s, 6H), 1.20 (s, 6H). ^{13}C-NMR (CDCl$_3$, 100 MHz) δ 181.4 [C], 164.4 [C], 127 [C], 113.4 [C], 83.4 [CH$_2$, J^1_{C-F} = 164 Hz], 45.4 [CH$_2$], 42.2 [CH], 29.9 [2C], 27.5 [CH$_2$, J^2_{C-F} = 20 Hz], 24.7 [CH$_2$, J^3_{C-F} = 4.5 Hz], 23.4 [2CH$_3$], 16.9 [2CH$_3$], 11.5 [CH$_3$], 11 [CH$_3$]. HR-ESI(+)-MS m/z calcd for C$_{17}$H$_{27}$FN$_2$OS: 327.1901 [M+H]$^+$, found 327.1902.

(Z)-*N*-(3-(5-fluoropentyl)-4,5-dimethylthiazol-2(3H)-ylidene)-2,2,3,3-tetramethylcyclopropane-1-carboxamide (2d). This derivative was prepared using 400 mg of 4,5-dimethylthiazol-2-amine (3.12 mmol) and 528 mg of 5-bromo-1-fluoropentane (4.05 mmol). Purification by flash chromatography (heptane / ethyl acetate 8/2 v/v) afforded **2d** (60 mg, 6 %) as a white solid. R_f (heptane / ethyl acetate 2/1 v/v): 0.35. M.p.: 138.8 – 139.9 °C. ^{1}H-NMR (CDCl$_3$, 400 MHz) δ 4.46 (dt, 2H, J = 5.6 Hz, J^1_{H-F} = 47.6 Hz), 4.08 (t, 2H, J = 7.6 Hz), 2.16 (s, 3H), 2.14 (s, 3H), 1.83 - 1.71 (m, 4H), 1.60 (s, 1H), 1.51 - 1.48 (m, 2H), 1.33 (s, 6H), 1.20 (s, 6H) ppm. ^{13}C-NMR (CDCl$_3$, 100 MHz) δ 181.3 [C], 164.3 [C], 127.1 [C], 113.3 [C], 83.6 [CH$_2$, d, J^1_{C-F} = 164 Hz], 45.8 [CH$_2$], 42.2 [CH], 29.9 [2C], 29.8 [CH$_2$, d, J^2_{C-F} = 19 Hz], 28.1 [CH$_2$], 23.9 [2CH$_3$], 22.4 [CH$_2$, d, J^3_{C-F} = 5 Hz], 16.9 [2CH$_3$], 11.5 [CH$_3$], 11 [CH$_3$] ppm. HR-ESI(+)-MS m/z calcd for C$_{18}$H$_{29}$FN$_2$OS: 341.2057 [M+H]$^+$, found 341.2072.

(Z)-*N*-(3-((E)-4-fluorobut-2-en-1-yl)-4,5-dimethylthiazol-2(3H)-ylidene)-2,2,3,3-tetramethylcyclopropane-1-carboxamide (2e). This derivative was prepared using 120 mg of 4,5-dimethylthiazol-2-amine (0.94 mmol) and 228 mg of 4-fluorobut-2-en-1-yl 4-methylbenzenesulfonate (1.22 mmol). Purification by flash chromatography (heptane / ethyl acetate 9/1 v/v) afforded **2e** (27 mg, 10 %) as a white solid. R_f (heptane / ethyl acetate 2/1 v/v): 0.43. M.p.: 114.8 – 116.2 °C. ^{1}H-NMR (CDCl$_3$, 400 MHz) δ 5.94-5.89 (m, 1H), 5.66-5.63 (m, 1H), 4.89 (dd, 2H, J = 5.2 Hz, $J^1_{H\text{-}F}$ = 46.0 Hz), 4.80 (t, 2H, 4.4 Hz), 2.15 (s, 6H), 1.51 (s, 1H), 1.32 (s, 6H), 1.26 (s, 6H) ppm. ^{13}C-NMR (CDCl$_3$, 100 MHz) δ 180.3 [C], 164.3 [C], 128.5 [CH, d, $J^3_{C\text{-}F}$ = 12 Hz], 127.2 [C], 127.0 [CH, d, $J^2_{C\text{-}F}$ = 17 Hz], 113.4 [C], 82.2 [CH$_2$, d, $J^1_{C\text{-}F}$ = 163 Hz], 46.7 [CH$_2$], 42.1 [CH], 30.3 [C], 29.6 [C], 23.9 [2CH$_3$], 16.8 [2CH$_3$], 11.4 [CH$_3$], 10.9 [CH$_3$] ppm. HR-ESI(+)-MS m/z calcd for C$_{17}$H$_{25}$FN$_2$OS: 325.1744 [M+H]$^+$, found 325.1759.

(Z)-*N*-(3-(2-(2-fluoroethoxy)ethyl)-4,5-dimethylthiazol-2(3H)-ylidene)-2,2,3,3-tetramethylcyclopropane-1-carboxamide (2f). This derivative was prepared using 100 mg of 4,5-dimethylthiazol-2-amine (0.78 mmol) and 266 mg of 2-(2-fluoroethoxy)ethyl 4-methylbenzenesulfonate (1.02 mmol). Purification by flash chromatography (dichlormethane) afforded **2f** (87 mg, 32 %) as a white solid. R_f (heptane / ethyl acetate 2/1 v/v): 0.31. M.p.: 117.9 – 118.6 °C. ^{1}H-NMR (CDCl$_3$, 400 MHz) δ 4.47 (dt, 2H, J = 4.0 Hz, $J^1_{H\text{-}F}$ = 48.0 Hz), 4.25 (m, 2H), 3.81 (m, 2H), 3.64 (dt, 2H, J = 4.0 Hz, $J^2_{H\text{-}F}$ = 29.6 Hz), 2.19 (s, 3H), 2.13 (s, 3H), 1.49 (s, 1H), 1.31 (s, 6H), 1.19 (s, 6H) ppm. ^{13}C-NMR (CDCl$_3$, 100 MHz) δ 180.2 [C], 163.5 [C], 129.0 [C], 113.3 [C], 82.7 [CH$_2$, d, $J^1_{C\text{-}F}$ = 168 Hz], 70.2 [CH$_2$, d, $J^2_{C\text{-}F}$ = 19 Hz], 68.7 [CH$_2$], 46.6 [CH$_2$], 41.6 [CH], 30.7 [2C], 23.9 [2CH$_3$], 16.8 [2CH$_3$], 11.5 [CH$_3$], 11.3 [CH$_3$] ppm. HR-ESI(+)-MS m/z calcd for C$_{17}$H$_{27}$FN$_2$O$_2$S: 343.1850 [M+H]$^+$, found 343.1855.

(Z)-N-(3-(2-hydroxyethyl)-4,5-dimethylthiazol-2(3H)-ylidene)-2,2,3,3-tetramethylcyclopropane-1-carboxamide (3). This derivative was prepared using 2.0 g of 4,5-dimethylthiazol-2-amine (15.82 mmol) and 2.5 g of 3-bromoethanol (20.31 mmol). Purification by flash chromatography (heptane / ethyl acetate 1/2 v/v) afforded **3** (87 mg, 32 %) as a white solid. R_f (heptane / ethyl acetate 3/7 v/v): 0.32. Mp: 143.1 – 144.7 °C. ^{1}H-NMR (CDCl$_3$, 400 MHz) δ 4.26 (t, 2H, J = 4.8 Hz), 3.95 (t, 2H, J = 4.8 Hz), 2.16 (s, 3H), 2.15 (s, 3H), 1.46 (s, 1H), 1.30 (s, 6H), 1.19 (s, 6H) ppm. ^{13}C-NMR (CDCl$_3$, 100 MHz) δ 180.4 [C], 166.3 [C], 127.4 [C], 113.9 [C], 63.2 [CH$_2$], 49.5 [CH$_2$], 41.8 [CH], 30.5 [2C], 23.8 [2CH$_3$], 16.7 [2CH$_3$], 11.6 [CH$_3$], 11.3 [CH$_3$] ppm. HR-ESI(+)-MS m/z calcd for C$_{15}$H$_{24}$N$_2$O$_2$S: 296.1558 [M+H]$^+$, found 296.1552.

(Z)-N-(3-(2-(3-fluoropropoxy)ethyl)-4,5-dimethylthiazol-2(3H)-ylidene)-2,2,3,3-tetramethylcyclopropane-1-carboxamide (2g). To a solution of **3** (536 mg, 1.0 equiv.) in DMF (10 mL) was added NaH (52 mg, 1.2 equiv.). The reaction mixture was stirred at room temperature for 30 min and 2-fluoropropyl tosylate (420 mg, 1.0 equiv.) was added. The reaction mixture was heated at 50 °C overnight. Upon cooling to room temperature, water (50 mL) was added and the mixture was extracted with ethyl acetate (3 x 150 mL). The combined organic phases were washed with water (100 mL) and brine (15 mL), dried over sodium sulfate, filtered, and concentrated to dryness under vacuum. The residue was purified by flash chromatography on silica gel (heptane / ethyl acetate 8/2 v/v) to afford **2g** (60 mg, 10 %) as a white solid. R_f (heptane / ethyl acetate 2/1 v/v): 0.41. M.p.: 104.9 – 107 °C. ^{1}H-NMR (CDCl$_3$, 400 MHz) δ 4.46 (dt, 2H, J = 6.0 Hz, $J^1_{H\text{-}F}$ = 47.2 Hz), 4.24 (t, 2H, J = 5.2 Hz), 3.74 (t, 2H, J = 5.2 Hz), 3.51 (t, 2H, J = 6.4 Hz), 2.19 (s, 3H), 2.14 (s, 3H), 1.90 (dq^5, J = 6.0 Hz, $J^2_{H\text{-}F}$ = 25.6 Hz), 1.15 (s, 1H), 1.33 (s, 6H), 1.20 (s, 6H) ppm. ^{13}C-NMR (CDCl$_3$, 100 MHz) δ 181.3 [C],

164.3 [C], 128.2 [C], 112.5 [C], 80.9 [CH$_2$, d, J^1_{C-F} = 163 Hz], 68.3 [CH$_2$], 66.8 [CH$_2$, d, J^3_{C-F} = 5 Hz], 46.1 [CH$_2$], 42.2 [CH], 30.6 [CH$_2$, d, J^2_{C-F} = 20 Hz], 30.0 [C], 23.9 [2CH$_3$], 16.8 [2CH$_3$], 11.5 [CH$_3$], 11.2 [CH$_3$] ppm. HR-ESI(+)-MS m/z calcd for C$_{18}$H$_{29}$FN$_2$O$_2$S: 357.2007 [M+H]$^+$, found 357.2016.

(Z)-2-(2-(4,5-dimethyl-2-((2,2,3,3-tetramethylcyclopropane-1-carbonyl)imino)thiazol-3(2H)-yl)ethoxy)ethyl 4-methylbenzenesulfonate (4). This derivative was prepared using 250 mg of 4,5-dimethylthiazol-2-amine (1.92 mmol) and 955 mg of oxybis(ethane-2,1-diyl) bis(4-methylbenzenesulfonate) (2.31 mmol). Purification by flash chromatography (CH$_2$Cl$_2$ / acetone 98/2 v/v) afforded **4** (386 mg, 40 %) as a white solid. R$_f$ (dichloromethane): 0.27. M.p.: 112 – 114 °C. ^{1}H-NMR (CDCl$_3$, 400 MHz) δ 7.75 (d, 2H, J = 8.4 Hz), 7.33 (d, 2H, J = 8.4 Hz), 4.18 (t, 2H, J = 4.4 Hz), 4.08 (t, 2H, J = 4.4 Hz), 3.73 (t, 2H, J = 4.8 Hz), 3.56 (t, 2H, J = 4.8 Hz), 2.44 (s, 3H), 2.14 (s, 3H), 2.13 (s, 3H), 1.19 (s, 1H), 1.31 (s, 6H), 1.18 (s, 6H) ppm. ^{13}C-NMR (CDCl$_3$, 100 MHz) δ 181.3 [C], 164.2 [C], 144.8 [C], 132.8 [C], 129.8 [2CH], 128.4 [C], 127.7 [2CH], 112.4 [C], 68.9 [CH$_2$], 68.7 [CH$_2$], 68.4 [CH$_2$], 46.0 [CH$_2$], 42.2 [CH], 30.1 [2C], 23.9 [2CH$_3$], 21.5 [CH$_3$], 16.8 [2CH$_3$], 11.5 [CH$_3$], 11.3 [CH$_3$] ppm. HR-ESI(+)-MS m/z calcd for C$_{24}$H$_{34}$N$_2$O$_5$S$_2$: 495.1982 [M+H]$^+$, found 495.1966.

In vitro pharmacology data

Biological material

Binding assays and cAMP assays were performed using membrane fractions of CHO cells expressing recombinant human CB$_2$R or CB$_1$R (hCB$_2$R and hCB$_1$R respectively, DiscoveRx, USA). Mouse spleen was collected from male C57BL/6J mice, 8 months old (Charles River, Italy), at the Santa Lucia Foundation within the project: 'Ruolo del Sistema Endocannabinoide nei Processi Neurodegenerativi in modelli animali di Alzheime' by Mauro Maccarrone. Ethical approval was given by the Ministry of Health, n. 47/2014/PR (deadline 17 November 2019). Spleen was suspended in 50 mM of Tris-HCl (pH 7.4), then was homogenized in a Potter homogenizer and centrifuged at 1,000 g for 10 min.

Binding assays

Membrane aliquots containing 5 mg (CHOK1hCB1_bgal) or 1 mg (CHOK1hCB2_bgal) of membrane protein in 100 mL assay buffer (50 mM Tris-HCl, 5 mM MgCl$_2$, 0.1% bovine serum albumin (BSA), pH 7.4) were incubated at 30 °C for 1 h, in presence of 3.5 nM [^{3}H]CP55940 or 1.5 nM [^{3}H]CP55940 respectively. Incubation was terminated by rapid filtration performed on GF/C filters (Whatman International, UK), presoaked for 30 min with 0.25% PEI, using a Brandel harvester (Brandel, USA). Filter-bound radioactivity was determined by scintillation spectrometry using a Tri-Carb 2900 TR liquid scintillation counter (Perkin Elmer, USA). For mouse experiments, spleen were resuspended in 2 mM Tris-EDTA, 320 mM sucrose, 5 mM MgCl$_2$ (pH 7.4), then homogenized and centrifuged three times at 1,000 g (10 min). The supernatants were centrifuged at 18,000 g (30 min), and the pellets were resuspended in assay buffer (50 mM Tris-HCl, 2 mM Tris-EDTA, 3 mM MgCl$_2$, pH 7.4). These membrane fractions were used in rapid filtration assays with 400 pM of [^{3}H]CP55940. In all binding experiments, non-specific binding was determined in the presence of 1 mM of CP55940. Bound radioactivity was analyzed for K$_i$ using nonlinear regression analysis (Activity Base, ID Business Solution Limited, UK), with the K$_d$ values for [^{3}H]CP55940 determined from saturation experiments.

cAMP assays were performed using the cAMP-Nano-TRF detection kit (Roche Diagnostics, Germany). Cells were seeded 17–24 h prior to the experiment at a density of 3 x 10^4 cells per well in a black 96-well plate with flat clearbottom (Corning, Germany) and incubated in 5% CO_2 at 37 °C in a humidified incubator. The growth medium was exchanged with Krebs Ringer bicarbonate buffer with 1 mmol/L 3-isobutyl-1-methylxanthine (IBMX), 0.1% fatty acid-free BSA and incubated at 30 °C for 1 h. Agonist and forskolin (3.5 μM) were added to a final assay volume of 100 μL and the mixture was incubated for 30 min at 30 °C. The assay was stopped by the addition of 50 μL lysis reagent provided by the cAMP-Nano-TRF detection kit (Roche Diagnostics, Germany) and shaken for 2 h at room temperature. The time-resolved energy transfer was measured using an LF502 Nanoscan FLT (IOM, Germany), equipped with a laser as excitation source. cAMP content was determined from the function of a standard curve spanning from 10 to 0.13 nmol/L cAMP.

Early ADME data

Distribution coefficient (log D)

The applied methods for the determination of the distribution coefficient (log D) are derived from the conventional 'shake flask' method. Compound of interest is dissolved in DMSO and the solution is dispensed in aqueous phosphate buffer (25 mM, pH 7.4). A part of this solution is analyzed by measuring the UV absorption. The obtained optical density (reference) is equal to the concentration of the substance before partitioning. An exact amount of 1-octanol is added and the mixture is gently shaken for 2 h. The emulsion is allowed to stand overnight to be sure that the partition equilibrium is reached. The next day, the concentration of the substance in the aqueous phase is determined again by measuring the UV absorption. The procedure above is carried out at four different octanol/water ratios, two with a large volume of octanol for hydrophilic compounds (log D < 1) and two with a low volume of octanol for the lipophilic compounds (log D > 1). The distribution coefficient is calculated from the difference in concentration in the aqueous phase before and after partitioning over the ratio of the two phases.

Kinetic solubility (LYSA)

Kinetic solubility of the test compounds in 0.05 M phosphate buffer (pH 6.5) is determined by means of a miniaturized high throughput solubility assay using standard microtiter plates. First, lyophilized, dry samples (n = 2) of the test compounds are prepared from 10 mM solutions in DMSO by removing the DMSO in a vacuum centrifuge (1 h, r.t., Genevac Technologies, USA). Then, phosphate buffer is added and the probes are sonicated using an ultrasonication system (Covaris C-1000). Finally, the samples are filtered using a microtiter filter plate (0.65 μm, Millipore MSDV N65) and the filtrate is analyzed by RapidFire-MS/MS. Data are expressed in microgram per milliliter (μg/mL).

pKa calculation

For the pKa calculations the MOKA software (version 2.6, Molecular Discovery, UK) was applied. The underlying pKa model was fitted by Roche internal measured pKa values.[28]

Passive membrane permeability (PAMPA)[29]

PAMPA (Parallel Artificial Membrane Permeability Assay) is a screen which simulates passive permeability and thus, oral absorption of drugs in the small intestine by a three compartments model, from a donor compartment, through a lipid-infused artificial membrane into an acceptor compartment.

Read-out is the permeability constant Peff [10^{-6} cm/s] of the drug as well as the drug distribution [percent] into donor, acceptor and membrane compartments which can be retrieved by UV or LC/MS analytics using a standard protocol and software (PAMPA Evolution, Pion Inc., USA). Materials: Donor buffer: 0.05 M MOPSO, pH = 6.5, 0.5% (w/v) glycocholic acid; acceptor buffer: 0.05 M MOPSO, pH = 6.5; artificial membrane: Millipore filter (MAIPN4550) impregnated with 4.5 mL of a solution containing 10% (w/v) egg lecithin, 0.5% (w/v) cholesterol in dodecane. Method: Donor solution is prepared by dissolving 15 mL of a 10 mM drug solution in DMSO in 985 mL donor buffer. The solution is filtered (0.22 μm GP Millipore Express Plus) and analyzed for content (UV absorption at 250-500 nm in steps of 2 nm) and filled into the donor compartment on top of the artificial membrane. The acceptor compartment is at the same time filled with acceptor buffer. After 18-24 hours of incubation time, the drug content in the donor and acceptor solution is quantified by UV or LC/MS analytics.

Microsomal clearance[30]

For human or mice, pooled commercially available microsomal preparations from liver tissues are used to account for biological variance *in vivo* (pooled human microsomes, BD UltraPool HLM 150, batch 38289, BD Bioscience, USA; pooled male mouse microsomes C57BL/6J, batch 4339006, Corning Incorporated, USA). For the microsomal incubations, 96 deep well plates are applied, which are incubated at 37 °C on a TECAN (Tecan Group Ltd, Switzerland) equipped with Te-Shake shakers and a warming device (Tecan Group Ltd, Switzerland). The incubation buffer is 0.1 M phosphate buffer at pH 7.4. The NADPH generating system consists of 30 mM glucose-6-phosphate disodium salt hydrate; 10 mM NADP; 30 mM $MgCl_2.6H_2O$ and 5 mg/mL glucose-6-phosphate dehydrogenase (Roche Diagnostics) in 0.1 M potassium phosphate buffer pH 7.4. Test compound (1 mM) has been incubated with microsomes (0.5 mg/mL) and NADPH as cofactor in 96-well plates at 37 °C. After 1, 3, 6, 9, 15, 25, 35 and 45 min, 40 μL incubation mixtures are transferred and the reaction was stopped by adding acetonitrile (15 μL) containing internal standards. Samples are then cooled and centrifuged before analysis by LC/MS/MS. Log peak area ratios (test compound peak area/internal standard peak area) are plotted against incubation time using a linear fit. The calculated slope is used to determine the intrinsic clearance: Cl_{int} (μL/min per mg protein) = -slope (min^{-1}) x 1000/[protein concentration (mg/mL)]. Data are obtained from single experiments measured with multiple time-points.

Hepatocyte clearance[31]

For animals, hepatocyte suspension cultures are either freshly prepared by liver perfusion studies or prepared from cryopreserved hepatocyte batches. For human, commercially available, pooled (5-20 donors) cryopreserved human hepatocytes from non-transplantable liver tissues are used. For the suspension cultures, Nunc U96 PP-0.5 mL (Nunc Natural, batch 267245) plates are used, which are incubated in a Thermo Forma incubator from Fischer Scientific (Switzerland) equipped with shakers from Variomag® Teleshake shakers (Sterico, Switzerland) for maintaining cell dispersion. The cell culture medium is William's media supplemented with glutamine, antibiotics, insulin, dexamethasone and 10% FCS. Incubations of a test compound at 1 mM test concentration in suspension cultures of 10^6 cells/mL (~1 mg/mL protein concentration) are performed in 96 well plates and shaked at 900 rpm for up to 2 h in a 5% CO_2 atmosphere and 37 °C. After 3, 6, 10, 20, 40, 60 and 120 min, 100 μL of cell suspension in each well are quenched with 200 μL methanol containing an internal standard. Samples are then cooled and centrifuged before analysis by LC/MS/MS. Log peak area ratios (test compound peak area / internal standard peak area) or concentrations are plotted against incubation time and a linear fit made to the data with emphasis upon the initial rate of compound disappearance. The slope

of the fit is then used to calculate the intrinsic clearance: Clint (μL/min/1 x 10^6 cells) = -slope (min^{-1}) x 1000 / [1 x 10^6 cells].

Plasma protein binding[27,32]

Pooled and frozen plasma from selected species were obtained from commercial suppliers. The Teflon equilibrium dialysis plate (96-well, 150 μL, half-cell capacity) and cellulose membranes (12–14 kDa molecular weight cutoff) were purchased from HT-Dialysis (Gales Ferry, USA). Both biological matrix and phosphate buffer pH are adjusted to 7.4 on the day of the experiment. The reference substance is diazepam. The determination of unbound compound is performed using a 96-well format equilibrium dialysis device with a molecular weight cut-off membrane of 12 to 14 kDa. The equilibrium dialysis device itself is made of Teflon to minimize non-specific binding of the test substance. Compounds are tested in cassettes of 2-5 with an initial total concentration of 1000 nM, one of the cassette compounds being the positive control diazepam. Equal volumes of matrix samples containing substances and blank dialysis buffer (Soerensen buffer at pH 7.4) are loaded into the opposite compartments of each well. The dialysis block is sealed and kept for 5 h at a temperature of 37 °C and 5% CO_2 environment in an incubator. After this time, equilibrium will have been reached for the majority of small molecule compounds with a molecular weight of < 600. The seal is then removed and matrix and buffer from each dialysis is prepared for analysis by LC/MS/MS. All protein binding determinations are performed in triplicates. The integrity of membranes is tested in the HTDialysis device by determining the unbound fraction values for the positive control diazepam in each well. At equilibrium, the unbound drug concentration in the biological matrix compartment of the equilibrium dialysis apparatus is the same as the concentration of the compound in the buffer compartment. Thus, the percent unbound fraction (fu) can be calculated by determining the compound concentrations in the buffer and matrix compartments after dialysis as follows: %fu = 100 x buffer conc after dialysis / matrix conc after dialysis. The device recovery is checked by measuring the compound concentrations in the matrix before dialysis and calculating the percent recovery (mass balance). The recovery must be within 80% to 120% for data acceptance.

Stability in human and mouse plasma

Heparinized plasma (human or mouse) was spiked with compound **2f** and incubated for 5 h at 37 °C (5% CO_2). Samples were collected at different time points and stabilized by addition of an organic solvent. Following centrifugation, the concentration of the molecule in the supernatant was quantified by (LC-MS) in each sample and the percentage of **2f** remaining at each time point was calculated and reported.

P-glycoprotein assay[33]

The P-glycoprotein (P-gp) assay evaluates the ability of test compounds to be transported transcellularly as a P-gp substrate. The assay uses transfected LLC-PK1 cells (porcine kidney epithelial cells, obtained from the Netherlands Cancer Institute) expressing human or mouse P-gp, cultured on 96-well semi-permeable filter membrane plates, where they form a polarized monolayer with tight junctions, and act as a barrier between apical and basolateral compartments. P-gp is expressed in the apical-facing membrane of the monolayer (tightness confirmed using Lucifer yellow). For substrate testing the assay determines the unidirectional permeability (Papp) of a test compound by separately dosing to the apical (for A4B Papp) and basolateral (for B4A Papp) sides of the cell monolayer (that is, donor compartments) and measuring the movement of the compound into the

respective receiver compartments over a 3 h incubation at 37 °C. The effect of P-gp is measured by expressing the efflux ratio (ER) of the unidirectional A4B and B4A Papp values. The mean permeability (A4B and B4A Papp) is determined in the absence of P-gp via addition of the selective inhibitor zosuquidar at a concentration of 1 mM. The ER and mean Papp are then used to categorize compound properties regarding their degree of efflux and permeability.

In vitro metabolism

Chemicals

D-glucose 6-phosphate disodium salt (G6P), nicotinamide adenine dinucleotide phosphate (NADPH), glucose-6-phosphate dehydrogenase (G6PDH) from yeast, formic acid and a bicinchoninic acid (BCA) protein assay kit were purchased from Sigma-Aldrich (France). Analytical LC/MS grade solvents were used for UPLC–tandem mass spectrometry analyses (Thermo Fisher Scientific, France).

Rat and human liver microsomes

Pooled human liver microsomes (pHLMs) fully characterized for their protein content, P450 concentrations and catalytic activities were obtained from Corning (France) and stored at -80 °C prior to use. Liver microsomes from Wistar male rats were prepared by homogeneization of liver samples over ice in a 0.1 M aqueous Tris-HCl buffer pH 7.4 containing 1 mM EDTA and 0.2 M sucrose, followed by differential centrifugations according to Kremer's method.[34] Total microsomal proteins content was determined according to the method of BCA using serum albumin as standard. Stock solution of **2f** (10 mM) was freshly prepared on the day of use in acetonitrile/water (30/70 v/v) containing 1% (v/v) formic acid keeping the final acid concentration below 0.1% (v/v).

Catalytic Activity Assay

A mixture containing 1 mg of microsomal proteins (rat or human liver microsomes), a NADPH-generating system (5 mM G6P, 1 mM $NADP^+$, 2 UI/assay G6P-dehydrogenase, 200 μL), **2f** (100 μM) and 0.1 M aqueous potassium phosphate buffer pH 7.4 in a final volume of 1 mL was incubated for 60 min at 37 °C under gentle shaking. The reaction was stopped by the addition of acetonitrile (1 mL). The mixture was centrifuged at 4 °C for 5 minutes at 9000 g. The resulting supernatant was filtered (Vecta Spin Micro 0.2 mm, Whatman, France), and stored at -20 °C until analysis of the extracts by LC/MS-MS as described below. In control assays, the mixture was incubated without the NADPH-generating system or without microsomes to confirm the stability of the compound in the experimental conditions. The percentage of each metabolite was determined as a percentage of the total peak area. Enzymatic catalytic activities are expressed as a formation rate of each metabolite in nmol per mg of microsomal proteins per minute (nmol metabolite/mg/min).

LC/MS/MS metabolites identification

The main oxidative metabolites generated upon P450 oxidation in microsomal incubates were characterized by LC/MS in the positive mode using an Ion Trap LTQ VelosPro ion mass spectrometer equipped with an electrospray source (Thermo Fisher Scientific, France). The Ultimate 3000 UPLC system interfaced with the LTQ consisted of LC pumps (HPG3400RS series N°8041829), photodiode

array (DAD3000 Series N°8041519) UV detector and autosampler (WPS3000TRS Series N°8043592, Dionex-Thermo Fisher Scientific, France). Pressurized nitrogen was used as sheath gas with a flow rate of 25 units (arbitrary units for sheath gas pressure as defined by the manufacturer). The source voltage for electrospray ionization was 4.5 kV; capillary voltage was 38 V and capillary temperature was 275 °C. **2f** and its metabolites were separated on a reverse phase UPLC HSS C18, 1.8 µm, 2.1x100 mm column (Waters, France). The mobile phase consisted of A: H_2O containing 0.05% formic acid and B: acetonitrile containing 0.05% formic acid. A linear gradient from 20 to 100% of B in 10 min was applied to the column at a flow rate of 300 µL/min. The whole output of the LC column was introduced into the PDA detector (190-800 nm) before electrospray ionization probe of the LTQ. The full scan MS acquisition mode was set up to detect ions in the range of *m/z* 50-500. The MS was set up in the MS/MS mode for acquiring, isolating with a mass width of 1 amu and dissociating the ion *m/z*=343 (**2f**) and its main metabolites by Collision Induced Dissociation and in the ion trap using helium as the collision gas with an energy of 37%. Data acquisition and processing were performed with Xcalibur™ software (version 2.2) with the assistance of Mass Frontier™ software (version 7.0) for proposed fragmentation mechanisms (Thermo Fisher Scientific, France).

Radiochemistry

Radiosynthesis

Automated radiosynthesis of [^{18}F]**2f** from **4** was performed using a TRACERlab FX$_{FN}$ synthesizer (GE Healthcare, USA) equipped with a 501 HPLC Pump (Waters, USA) and a UV detector K-2501 (Knauer, Germany). No carrier-added [^{18}F]fluoride ion is produced via the ^{18}O(p, n)^{18}F nuclear reaction by irradiation of a 2 mL [^{18}O]water (> 97% enriched, CortecNet, France) target with an IBA Cyclone-18/9 (IBA, Belgium) cyclotron. [^{18}F]F$^-$ (20-30 GBq) is trapped on an ion exchange resin QMA light (Waters) and eluted with a solution of K_2CO_3 (2 mg) in a mixture of CH_3CN (0.7 mL) and H_2O (0.3 mL) containing Kryptofix-222 (12-15 mg). The resulting complex is azeotropically dried upon heating at 60 °C for 7 min under vacuum and a stream of helium followed by heating at 120 °C for 5 min under vacuum only. A solution of precursor **4** (4 mg) in DMSO (0.7 mL) is added and the mixture is heated at 120 °C for 5 min. Upon cooling to 50 °C, the crude is diluted with a solution of H_2O/CH_3CN/TFA (2 mL, 55/45/0.1 v/v/v) and passed through an alumina cartridge (Sep-Pak Alumina-N, Waters, USA). The cartridge is further washed with the same solution (2 mL) and the combined phases are injected for purification. Semi-preparative HPLC was performed on a reverse phase Zorbax C18 column (250 x 9.4 mm, 5 µm, Agilent, USA) using a mixture of H_2O/CH_3CN/TFA (55/45/0.1 v/v/v, 5 mL/min) as eluent with gamma and UV (λ = 280 nm) detection. The collected peak (t_R = 9-9.5 min) of [^{18}F]**2f** is diluted with water (20 mL) and loaded on a C18 cartridge (Sep-Pak C18, Waters). The cartridge is rinsed with water (10 mL) and the product is eluted with ethanol (2 mL) and further diluted with aq. 0.9 % NaCl (18 mL). Ready-to-inject [^{18}F]**2f** was obtained within 45 min from end of beam (EOB) in 15 ± 5% (n = 8) radiochemical yield (RCY).

Quality Control

Quality control was performed on three consecutive runs for each batch of [^{18}F]**2f** using a 717$_{plus}$ Autosampler HPLC system equipped with a 1525 binary pump and a 2996 photodiode array detector (Waters) and a Flowstar LB 513 (Berthold, France) gamma detector. The system was monitored with the Empower 3 (Waters) software. HPLC were realized on a reverse phase analytical Symmetry C18 (150 x 3.9 mm, 5 µm, Waters) column using a mixture of H_2O/CH_3CN/PicB7$^®$ (50/50/0.1 v/v/v, 2 mL/min) as eluent. UV detection was performed at 302 nm. Identification of the peak was assessed by

comparing the retention time of [^{18}F]**2f** with the retention time of the non-radioactive reference **2f** (t_R^{ref}). For acceptance, the retention time must be within the $t_R^{ref} \pm 10\%$ range. Radiochemical and chemical purities were calculated as the ratio of the area under the curve (AUC) of the **2f** peak over the sum of the AUCs of all other peaks on gamma and UV chromatograms respectively. Radiochemical and chemical purities are the mean values of three consecutive runs. Molar activity was calculated as the ratio of the activity of the collected peak of [^{18}F]**2f** (Capintec®, Berthold) over the molar quantity of **2f** determined using calibration curves. Molar activity is calculated as the mean value of three consecutive runs. All these controls were repeated two hours after the end of the synthesis to verify the stability in solution of [^{18}F]**2f**.

In vivo biodistribution and metabolic profile of [^{18}F]2f in rats

Animals

All animal experiments were conducted according to the European directive 2010/63/EU on the protection of animals used for scientific purposes. Protocols were approved by the local ethic committee (CETEA DSV n°: 44). Male Wistar rats (320± 13 g, Janvier, France) were housed under standard 12 h : 12 h light/dark conditions (lights on from 8:00 a.m. to 8:00 p.m.) in a temperature- and humidity-controlled room. Animals have access to food and water ad libitum. Before using rats for experiments, they were allowed to adapt to the animal facility for one week.

Autoradiography

A rat was anaesthetized and maintained under anesthesia with 4-5% of isoflurane and perfused transcardially with saline solution (aq. 0.9% NaCl). Organs were rapidly excised and frozen in isopentane precooled in liquid nitrogen (-50 °C) and then stored at -80 °C until use. Frozen spleen sections (12 μm thick) were cut at -20°C using a cryostat (Leica, Germany). Sections were absorbed on SuperFrost Plus slides (Menzel, USA) and stored at -80 °C until use. For the experiment, the slices were thawed on ice for 10 min before conditioning in incubation Tris buffer (Trizma 50 mM, NaCl 120 mM, pH = 7.4). Slices were then incubated for 20 min with Tris buffer containing [^{18}F]**2f** (111 MBq, 1.0 nmol, 0.56 Bq/mL) alone or [^{18}F]**2f** (111 MBq, 1.0 nmol, 0.56 Bq/mL) in mixture with non-radioactive reference **2f** (20 μM) or GW405833 (20 μM). Slices were then washed twice for 2 min and once for 10 sec with cold (4 °C) Tris buffer. Tissue sections were then exposed on a Phosphor-Imager screen overnight (Storm 860, Molecular Dynamics, GE Medical Systems, USA). Autoradiograms were then scanned and analyzed using the ImageJ (NIH) and Optiquant (Packard, USA) softwares. The radioactivity concentration in the autoradiograms was expressed in digital light units per square millimeter.

Biodistribution

Healthy rats were injected via the tail vein with 9-12 MBq of [^{18}F]**2f** (20 MBq/mL, 0.2-0.5 nmol). The animals, under gaseous isoflurane anesthesia, were sacrificed by sampling of whole blood from the abdominal aorta at 5, 15, 30 and 60 min after injection (n = 4). Blood and some organs (brain, muscle, lung, heart, liver, kidney and spleen) were collected, weighed and counted for radioactivity using a gamma counter. Radioactivity concentration in the organs was expressed as percent of the injected dose per gram of tissue (% ID/g).

Pre-treatment experiment

Controls animals (n = 4) were injected *via* the tail vein with vehicle (0.9% NaCl$_{aq}$ containing < 5% EtOH) 15 min before radiotracer injection (9-12 MBq of [^{18}F]**2f**, 20 MBq/mL, 0.2-0.5 nmol). Pre-treated animals (n = 4) were injected either with **2f** (1.5 mg/kg in solution in 0.9% NaCl$_{aq}$ containing < 5% EtOH), GW405833 (1.5 mg/kg in solution in 0.9% NaCl$_{aq}$ containing < 5% EtOH) or NIDA41020 (1.5 mg/kg in solution in 0.9% NaCl$_{aq}$ containing < 5% EtOH) 15 min before radiotracer injection (9-12 MBq of [^{18}F]**2f**, 0.2-0.5 nmol). The animals, under gaseous isoflurane anesthesia, were sacrificed by sampling of whole blood from the abdominal aorta at 30 minutes after injection. Blood and some organs (brain, muscle, lung, heart, liver, kidney, spleen) were collected, weighed and counted for radioactivity using a gamma counter. Radioactivity concentration in the organs was expressed as percent of the injected dose per gram or tissue (%ID/g) normalized by the %ID/g of blood (*i.e.* (%ID/g tissue) / (%ID/g blood)). Statistical analyses are performed by one-way anova/multiple comparison.

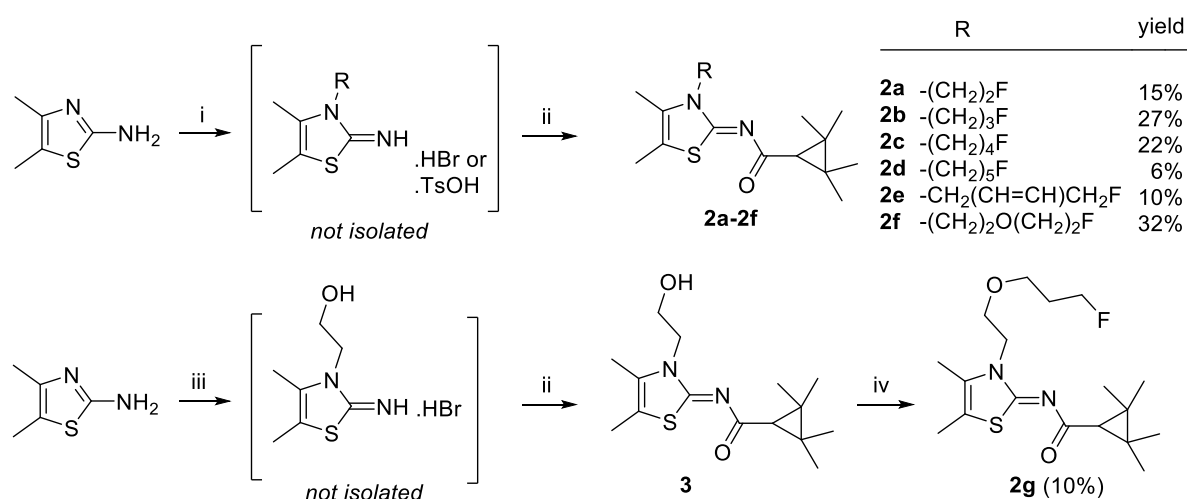*Radiometabolites analysis in plasma*

Rats (n = 8) were injected via the tail vein with 42 ± 15 MBq (90 MBq/mL, 0.38 nmol) of [^{18}F]**2f**. Blood samples were collected from the abdominal aorta at 5, 15, 30 and 60 min after injection and immediately centrifuged at 4 °C for 5 min at 3,000 g to obtain cell-free plasma. The radioactivity in the plasma samples (500 µL) was measured in a cross-calibrated gamma-counter (Cobra Quantum D5003; Perkin-Elmer, France) and expressed in Becquerels. All the values were corrected for fluorine-18 decay (109.8 minutes). For the radiometabolite analysis, arterial plasma samples (500 µL) were counted, deproteinated with 700 µL of acetonitrile, and centrifuged at 4 °C for 2 min (3,000 g). The radioactivity in the resulting precipitate was measured for calculating the percentage recovery of radioactivity in the acetonitrile extract. The whole supernatant was injected onto the radio-HPLC system equipped with a quaternary gradient pump, an ASI100T autosampler and a UVD170U UV-Vis detector (Dionex S.A., France) online with a LB-509 radioisotope detector (MX Z500 cell; Berthold, France) and a fraction collector. [^{18}F]**2f** and its radiometabolites were separated using a 5 µm, 10 x 250 mm, C18 SunFire preparative column (Waters, France). The mobile phases consisted of 0.1% trifluoroacetic acid in water (A) and 0.1% trifluoroacetic acid in acetonitrile (B). A linear gradient from 20% to 50% of B in 10 min was applied at a flow rate of 5 mL/min. The radioactivity in all the collected fractions (every 15 sec) was measured in the gamma counter. Data acquisition and processing were performed with Chromeleon software (version 1.0; Dionex, France). The radioactivity due to unchanged [^{18}F]**2f** was expressed as a fraction of the total radiolabeled peak areas. The percentages of unchanged [^{18}F]**2f** in plasma as a function of time were fitted by a nonlinear regression analysis (OriginPro software version 8.5; OriginLab, USA) using a standard biexponential decay equation.

RESULTS AND DISCUSSION

Chemistry

The seven fluorinated analogs of A-836339 (**1**) were synthesized following the procedures depicted in Scheme 1. Six (**2a-f**) out of seven analogs were synthesized according to a two steps procedure from commercially available 4,5-dimethylthiazol-2-amine following the same approach used by Moldovan *et al.*.[26] Mimicking the methoxyethyl chain of parent compound A-836339, different lengths of

fluorinated side chains were grafted to explore their influence on the binding affinity and selectivity for CB_2R. Among them, an alkene analog (compound **2e**) has also been tested to investigate the influence of the rigidity of the side chain whereas PEGylated derivatives (compounds **2f** and **2g**) were designed to balance water solubility. The first step of *N*-alkylation was carried out using different fluorinated alkyl chains either commercially available (for compound **2c** and **2d**) or synthesized according to procedure described in the literature.[35-38] The resulting hydrobromine or tosylated salt of the corresponding thiazole imine derivatives were not isolated and used directly in the next step. Final coupling reaction with 2,2,3,3-tetramethylcyclopropane-1-carboxylic acid in the presence of benzotriazole-1-yl-oxy-tris(dimethylamino)phosphonium (BOP) as coupling agent and triethylamine afforded compounds **2a-f**. Despite the low to moderate yields (6-32%), this straightforward approach proved to be robust enough to synthesize a small library of compound in a time-effective manner. Considering the dissymmetry of the fluorinated alkoxy chain of compound **2g**, a three steps procedure was realized for the preparation of this derivative (Scheme 1). 4,5-Dimethylthiazol-2-amine was alkylated with 2-bromoethan-1-ol in similar conditions as for the other derivatives. The resulting thiazole imine hydrobromate was not isolated and used directly in the coupling reaction with 2,2,3,3-tetramethylcyclopropane-1-carboxylic acid to give compound **3** in 47% yield over two steps. *O*-alkylation of the primary hydroxyl group with 3-fluoropropyl tosylate in the presence of sodium hydride afforded compound **2g** in 10% overall yield.

	R	yield
2a	-$(CH_2)_2F$	15%
2b	-$(CH_2)_3F$	27%
2c	-$(CH_2)_4F$	22%
2d	-$(CH_2)_5F$	6%
2e	-$CH_2(CH=CH)CH_2F$	10%
2f	-$(CH_2)_2O(CH_2)_2F$	32%

Scheme 1. Synthesis of compounds **2a-g**. *Reagents and conditions:* i) fluorinated alkylating agent, 85 °C, overnight; ii) 2,2,3,3-tetramethylcyclopropane-1-carboxylic acid, BOP, Et₃N, CH_2Cl_2, r.t., 12h; iii) 2-bromoethan-1-ol, 85 °C, 12h; iv) $TsO(CH_2)_3F$, NaH, DMF, 50 °C, overnight.

In vitro Pharmacology data

Fluorinated analogs **2a-g** of A-836339 (**1**) were evaluated in both human and mouse CB_2R as well as in human CB_1R binding assays (Table 1). Furthermore, their functional activity and efficacy was assessed in human CB_2, mouse CB_2 and in human CB_1 cyclic adenosine monophosphate (cAMP) assays according to a procedure described in the literature.[39] All compounds display high binding affinities for the human CB_2 receptor. Except for compound **2a** containing only two carbon atoms between the thiazole core and the fluorine (K_i = 2 nM), all other derivatives are subnanomolar binders (K_i = 0.1-0.3 nM) with ethoxyethyl thiazole **2f** being among the best compounds, in the same range as

the reference compound A-836339 (K_i = 0.3 nM). Elongating the fluorinated alkyl residue increases the binding affinity, a result also observed by Moldovan *et al.*.[26] Importantly, no species differences between human and mouse have been noted as compounds **2a-g** are also highly potent binders for the mouse CB_2 receptor. Elongating the fluorinated side chain still improves the binding affinity down to subnanomolar values on the mouse CB_2R. Again ethoxyethyl thiazole **2f** is among the ligands with the highest affinity (mouse CB_2R K_i = 0.1 nM).

The binding selectivity towards the human CB_1 receptor, measured as the ratio of the K_i for CB_1R over the K_i for CB_2R, is at least 130 fold and comparable to the selectivity ratios measured by Moldovan *et al.*.[26] Elongating the fluorinated side chain also increases the binding affinity for the CB_1R in a similar way as for the CB_2R thus leveling the selectivity throughout the series. The binding selectivity is for most of the compounds except **2b** one order of magnitude lower than the selectivity observed for reference compound A-836339 (2137 vs 130-825). If the length of the side chain plays a key role in the binding affinities over the two receptors, the fluorine atom seems to have a detrimental effect on the selectivity by increasing the affinity over CB_1R in a more important manner than for CB_2R. Surprisingly, the fluoropropyl derivative **2b** displays a selectivity around one order of magnitude higher than the rest of the series (2813 vs 130-825), comparable to A-836339. This result has also been observed by Moldovan *et al.*.[26]

Regarding the functional activity, compounds **2a-g** are full agonists and possess picomolar EC_{50} values for the human CB_2 receptor (Table 2). Functional selectivity against the CB_1 receptor is even higher than binding selectivity, reaching hCB_1 cAMP EC_{50} / hCB_2 cAMP EC_{50} ratios higher than 10^6 in the case of fluoroethyl derivative **2a**. Also with respect to functionality, no species differences exist and all compounds are full agonists of the mouse CB_2 receptor, too. Human and mouse EC_{50} values are comparable. Overall, ethoxyethyl derivative **2f** combines high potency and functional selectivity with highest binding affinity for both human and mouse CB_2 receptor.

Table 1. Binding affinity and selectivity of A-836339 and its fluorinated analogs **2a-g**.

Compound	hCB_2 K_i (nM)	hCB_1 K_i (nM)	hCB_1 K_i / hCB_2 K_i	mCB_2 K_i (nM)
A-836339	0.3	423	2137	0.9
2a	2.4	1979	825	3.5
2b	0.3	844	2813	1.3
2c	0.2	91	455	0.3
2d	0.1	13	130	0.1
2e	0.1	39	390	0.3
2f	0.1	30	300	0.1
2g	0.1	26	260	0.3

Table 2. Functional activity and selectivity of A836339 and its fluorinated analogs **2a-g**.

Compound	hCB_2: cAMP EC_{50} (nM), efficacy (%)	hCB_1 cAMP EC_{50} (nM), efficacy (%)	hCB_1 cAMP EC_{50} / hCB_2 cAMP EC_{50}	mCB_2 cAMP EC_{50} (nM), efficacy (%)
A-836339	0.01, 95	2256, 121	158287	0.062, 98

2a	0.05, 91	>10^4, 19	>10^6	0.133, 95
2b	0.02, 94	682, 56	35127	0.066, 98
2c	0.06, 96	56, 100	862	0.094, 97
2d	0.02, 94	4, 97	171	0.060, 98
2e	0.12, 93	77, 92	621	0.242, 96
2f	0.03, 96	18, 95	599	0.059, 98
2g	0.02, 96	11, 95	473	0.128, 97

Early ADME profiles.

To assess the suitability of fluoro thiazole derivatives **2a-g** as PET tracers, early ADME data were generated (Table 3). Special emphasis was put on lipophilicity, membrane permeation properties and metabolic stability in microsomes and hepatocytes as these parameters are of paramount relevance for PET tracers targeting the central nervous system.[40] The optimal range of calculated physicochemical values predicting brain permeability includes a molecular weight (MW) < 500 g/mol, a small topological surface area (TSPA, < 75 Å^2) and a number of hydrogen-bond donors (HBD) below 1. Compounds **2a-g** meet all these criteria. None of them contains a HBD, the TSPA is between 21 and 29 Å^2 and the molecular weight does not exceed 357 g/mol. Lipophilicity needs to be balanced to enable membrane permeability. According to Lipinski's rule, lipophilicity should be below 5 but Ryckmans *et al.* showed on a series of CB$_2$R agonists that ideal values of clogP are between 2 and 4.[41] Calculated lipophilicity values (Kow clogP) and experimentally generated octanol/water distribution coefficients (log D) look most favorable for the ethoxyethyl derivative **2f** (log D = 3.5). Most of other compounds display higher lipophilicity which may account for stronger interactions with plasma proteins and lower free fraction of tracer available for the CB$_2$ receptor binding. Importantly, none of the CB$_2$R ligands **2a-g** is charged at physiological pH since their basic pK$_a$ values are all below 5. Kinetic solubility (LYSA) is highest for compound **2f**, predicting good bioavailability properties for this analog. Passive membrane permeability was assessed using the parallel artificial membrane permeability assay (PAMPA) model.[29] The permeation coefficient P_{eff} is generally > 10^{-6} cm/s, except for compound **2c**, and the molecules partition is predominant into the membrane (%Mem. = 53-79%) and reach the acceptor compartment (%Acc. = 1-5%). Compound **2f** shows again one of the best results with 4% of the molecule reaching the acceptor compartment, underlining its promising capacity to cross biological barriers. A fast clearance is also desirable for a rapid wash out of non-target bound PET tracer to reduce the non-specific signal. Therefore, the clearance rates of CB$_2$R ligands **2a-g** were determined in co-incubation experiments with liver microsomes. For all molecules clearance in human microsomes was high and increased with the length of the fluorinated side chain. In mouse microsomes, the clearance was > 1000 µL/min/mg for all molecules.

Table 3. Calculated physicochemical and early ADME properties with relevance for good *in vivo* performance for A-836339 and fluorinated analogs **2a-g**.

Compound	MW (g/mol)	TSPA (Å^2)	Kow clogP	LogD (pH 7.4)	LYSA (μg/mL)	pKa	PAMPA P_{eff} (10^{-6} cm/s), %Acc./%Mem./ %Don.	Microsomal cl. (human/mouse) (μL/min/mg)
A-836339	310.5	29	2.97	3.79 ± 0.07	7.1 ± 1.6	4.82 ± 0.02	4.34 ± 2.85 5 / 62 / 33	165 / > 1000
2a	298.4	23	3.68	3.44 ± 0.07	0.9 ± 0.1	4.55 ± 0.01	1.36 ± 0.23 3 / 53 / 44	107 / > 1000
2b	312.4	22	4.17	3.64 ± 0.02	0.8 ± 0.1	4.71 ± 0.01	5.81 ± 1.5 4 / 78 / 18	189 / > 1000
2c	326.5	22	4.66	4.00 ± 0.09	0.3 ± 0.1	4.84 ± 0.01	0.72 ± 0.2 1 / 63 / 36	262 / > 1000
2d	340.5	22	5.15	3.59 ± 0.05	<0.2	4.87 ± 0.02	n.d.	345 / > 1000
2e	324.5	21	4.44	3.79 ± 0.05	0.7 ± 0.1	4.56 ± 0.01	2.15 ± 0.6 2 / 79 / 19	307 / > 1000
2f	342.5	29	3.40	3.53 ± 0.05	2.6 ± 0.2	4.93 ± 0.01	3.82 ± 1.5 4 / 66 / 30	206 / > 1000
2g	356.5	29	3.89	3.82 ± 0.04	0.2 ± 0.1	4.88 ± 0.01	1.23 ± 0.3 2 / 67 / 31	376 / > 1000

With the most favorable physicochemical and pharmacological properties, ethoxyethyl thiazole **2f** was selected for further profiling towards its utility as PET tracer (Table 4). Metabolic stability in human and mouse hepatocytes was assessed and the high clearance in both species already seen in microsomes could be confirmed. Plasma free fraction (2.6% and 5.9% for human and mouse respectively) which is an important parameter to influence brain entry and non-specific signal is in a favorable range considering that the endogenous ligands of this receptor are tightly protein bound fatty acid derivatives. In comparison, compound **2c** chosen by Moldovan *et al.*[26] displays a log *D* of 4.00 and is more likely to bound to plasma proteins. Compound **2f** was furthermore assessed for its stability in both human and mouse plasma. After incubation for 5 h at 37 °C the compound was found to be fully intact. Importantly **2f** is not a substrate of the P-glycoprotein (P-gp) efflux transporter which is highly expressed at the blood brain barrier. Extraction ratios (ER) are 1.2 for both human and mouse

P-gp. In summary, the CB$_2$R ligand ethoxyethyl thiazole **2f** meets all criteria with regard to pharmacological, physicochemical and early ADME properties for becoming a successful PET tracer and was therefore selected for labeling with fluorine-18.

Table 4. Additional ADME properties of ethoxyethyl thiazole **2f**.

Compound	Hepatocyte clearance (human/mouse) (µL/min/Mio cells)	Plasma protein binding: Free fraction (human/mouse) (%)	Stability in plasma % remaining after 5 h incubation @ 1 µM at 37 °C (human/mouse)	P-glycoprotein mediated efflux extraction ratio (human/mouse)
2f	> 200 / > 200	2.64 ± 0.07 / 5.9 ± 0.14	102 / 105	1.2 ± 0.2 / 1.2 ± 0.2

In vitro metabolism of 2f.

To further explore the potential of compound **2f** as a PET tracer, LC/MS metabolic profiles upon human and rat liver microsomal incubation were determined (Figure 3). A total of six main metabolites (namely M1 to M6) of **2f** (*m/z* [M+H]$^+$ 343), generated by cytochrome P$_{450}$-dependant hydroxylations, di-hydroxylations and an *O*-dealkylation, were identified in human liver microsomes as follows: M1, M2 and M5 (*m/z* 359), M3 and M6 (*m/z* 375) and M4 (*m/z* 297) respectively. In rat liver microsomes, the same three main hydroxylated metabolites (*m/z* 359) M1, M2 and M5 were observed but in different proportions than in human microsomes. Indeed, M1 (t_R = 5.78 min) is the major mono-hydroxylated metabolite in human microsomes whereas M5 (t_R = 4.55) is predominant in rat microsomes. Regarding the di-hydroxylated metabolites (*m/z* 375), at least seven different compounds were observed in rat microsomes, including M3 (t_R = 5.28 min) and M6 (t_R = 3.90 min). These differences suggest strong species dependence for the biotransformation of **2f** with more degradation observed in the rat model. The non-metabolized compound **2f** (t_R = 6.41 min) was still observed in high proportion after human microsomal incubation whereas rat microsomal incubation showed almost total metabolization indicating higher stability of **2f** in human microsomal conditions. Together with the good stability in human plasma, compound **2f** shows very promising *in vitro* data to be developed as a PET tracer in human.
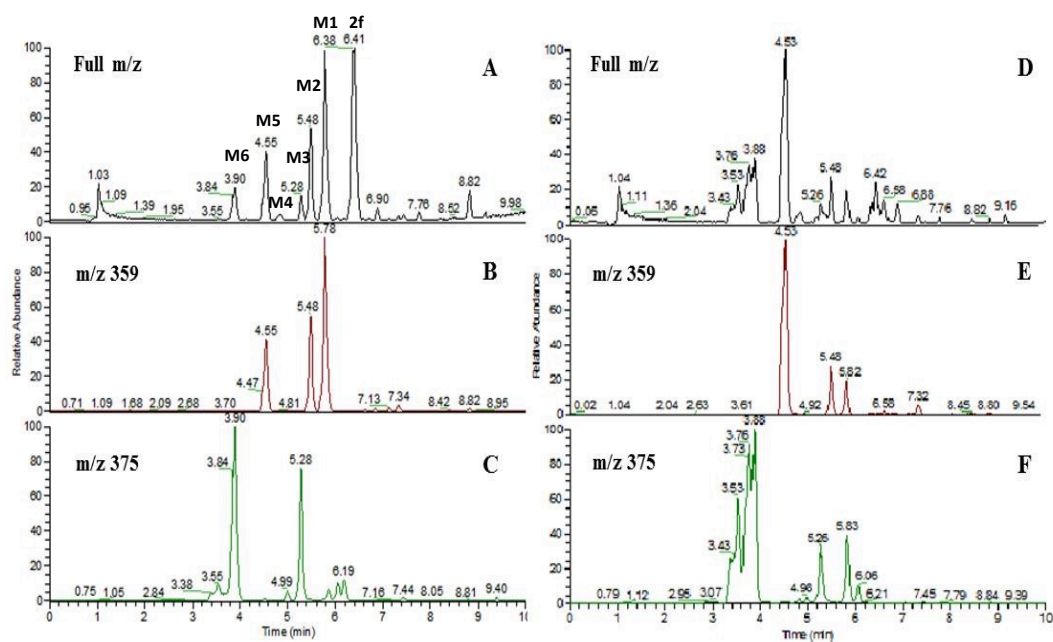
Figure 3. Representative LC/MS chromatograms of human (left) and rat (right) liver microsomal extracts. Full m/z chromatograms (A and D for human and rat, respectively) and selected mass chromatograms (m/z = 359, B and E for human and rat, respectively; m/z = 375, C and F for human and rat, respectively) are presented.

To further understand the mechanisms involved in the biotransformation of compound **2f**, MS^2 and MS^3 experiments were carried out on the six main metabolites and the results are presented in Table S1 (see supplementary data). The major fragmentations occurring on compound **2f** are depicted in Figure 4. The main MS^2 fragments extracted from parent compound **2f** (*m/z* 343*)* resulted from the loss of the tetramethylcyclopropane-1-carboxamide group (*m/z* 245 and 219) followed by the loss of the *O*-fluoroethyl chain (*m/z* 155) or the *N*-fluoroethoxyethyl moiety (*m/z* 129). A ring opening process was also observed with parent compound **2f**, resulting in the formation of a sulfonium metabolite (*m/z* 192). The mass spectrum of M1, M2 and M5 exhibited a molecular ion at *m/z* 359, higher than the molecular ion for **2f** (+ 16 amu), which is consistent with the insertion of an oxygen atom in the parent molecule. Data dependent scan MS^3 experiments on the main MS^2 fragment of M1 and M2, *m/z* 235 suggested that hydroxylation probably occurred on one of the methyl substituents of the dimethylthiazole core and not on the tetramethylcyclopropane ring. On the opposite, similar experiment on the same fragment of M5, the more polar hydroxylated metabolite, is consistent with the insertion of an oxygen atom probably occurring on another part of the molecule. The preservation of the fragments at *m/z* 219 and 155 suggested that the more likely position may be the tetramethylcyclopropane moiety. M3 and M6 exhibited a molecular ion at *m/z* 375, higher than the molecular ion for **2f** (+ 32 amu), which is consistent with the insertion of two oxygen atoms in the parent molecule. MS^2 and MS^3 experiments suggested in the case of M6, both hydroxylation reactions occurred on the methyl groups of the thiazole ring (*m/z* 261) whereas both the thiazole and the cyclopropane ring were hydroxylated in the case of M3. Fragmentation of M4 (*m/z* 297) is consistent with the loss of the fluoroethyl group by *O*-deethylation in the parent molecule leading to a loss of 47 amu in the fragment ion (*m/z* 173).
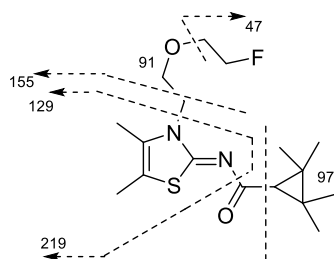
Figure 4. Major fragmentations occurring on compound **2f**.

Given the information collected with MS^2 and MS^3 spectra after incubation of **2f** with human liver microsomes, metabolic pathways can be proposed (Figure S1, see supplementary data). Most metabolites result from the hydroxylation of one of the six methyl groups of the parent compound. Oxidation at the sulfur or the nitrogen atoms also occurs. All these metabolites still bear the fluorinated side chain and would therefore be potential radiometabolites in the case of a PET tracer labeled with fluorine-18. Radiometabolites crossing the blood brain barrier may interfere with PET quantification and identifying them is of prime importance. Furthermore correcting the arterial input function is mandatory for compartmental modeling in the absence of a region of reference. *O*-deethylation and *N*-dealkylation also occur to a lesser extent, leading to the formation of a non-radioactive metabolite and to the loss of the fluorinated side chain. The fluoroethyl chain is known to be rapidly oxidized into fluoroacetaldehyde and fluoroacetic acid and eventually lead to defluorination and significant bone uptake.[42,43] However, dealkylation is not the major metabolic pathway of the degradation of **2f** by microsomes and should not be detrimental degradation for PET imaging.

Radiochemistry.

Synthesis of the corresponding tosylated precursor **4** for fluorine-18 labeling was achieved in two steps from 4,5-dimethylthiazol-2-amine (Scheme 2). *N*-alkylation with diethylene glycol ditosylate afforded the tosylated salt of the corresponding thiazole imine which was isolated. Coupling reaction with 2,2,3,3-tetramethylcyclopropane-1-carboxylic acid in the presence of BOP and trimethylamine afford the precursor **4**. The tosylated side chain proved to be long enough to prevent intramolecular cyclisation between the nitrogen atom of the amide moiety and the terminal leaving group. Compound **4** was obtained in a moderate yield of 40% over two steps and proved to be stable at room temperature overtime.
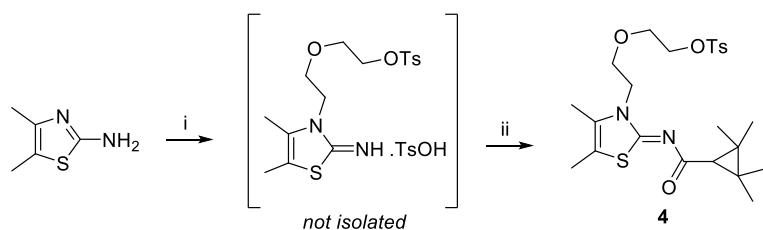
Scheme 2. Synthesis of precursor **4** for fluorine-18 labeling. *Reagents and conditions:* i) TsO(CH$_2$)$_2$O(CH$_2$)$_2$OTs, 85 °C, 12h; ii) 2,2,3,3-tetramethylcyclopropane-1-carboxylic acid, BOP, Et$_3$N, CH$_2$Cl$_2$, r.t., 12h.

Radiolabeled [^{18}F]**2f** was prepared using a GE TRACERlab^{TM} FX$_{FN}$ synthesizer by aliphatic nucleophilic substitution of the tosylate group on precursor **4** using dry [^{18}F]fluoride in the presence of potassium carbonate and Kryptofix-222 (Scheme 3). Reaction was carried out in DMSO at 120 °C for 5 minutes. Prolonged time (10 minutes) or higher temperature (160 °C) did not result in higher conversion into the desired radiotracer. A two steps purification process was performed by filtration through a Sep-Pak Alumina N cartridge to remove unreacted fluoride followed by reverse phase semi-preparative HPLC (Figure S2, see supplementary data). No significant other radioactive compound was observed during the purification, witnessing the good stability of the thiazole scaffold under nucleophilic conditions. Only one major non-radioactive degradation product was observed on the UV chromatogram (t_R = 5 min) probably corresponding to the hydrolysis of the tosylate moiety under basic conditions. Final solid phase formulation on a C18 cartridge afforded ready-to-inject [^{18}F]**2f** in 15 ± 5% (n = 8) RCY within 45 minutes. Quality control by reverse phase analytical HPLC showed radiochemical purity above 98% and a chemical purity above 95% based on UV-chromatogram (λ = 302 nm). [^{18}F]**2f** was obtained with a satisfying molar activity (MA) of 110 ± 30 GBq/µmol (EOB, n = 8). [^{18}F]**2f** proved to be stable in solution at least 2 hours after production upon controlling the integrity of the sample by analytical HPLC.
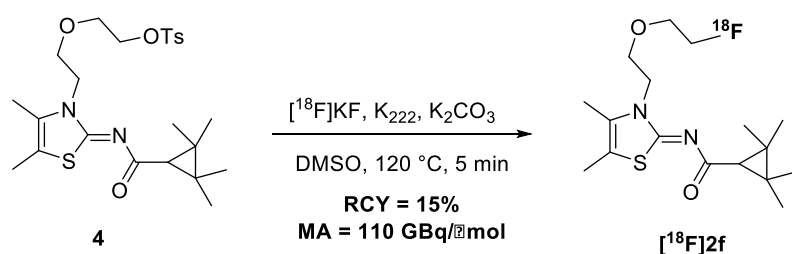
Scheme 3. Radiosynthesis of [^{18}F]**2f** from precursor **4**.

Autoradiography

[^{18}F]**2f** was firstly evaluated *ex vivo* by autoradiography on a healthy rat (Wistar) spleen, a CB$_2$R-rich organ under physiological conditions. The spleen sections were recovered from a single animal which was perfused with 0.9% NaCl$_{aq}$ solution to overcome the non-specific radioactive signal coming from the residual blood in the organ. Tissue sections were incubated with [^{18}F]**2f** alone (111 MBq, 1.0 nmol, 0.56 MBq/mL) or with either 20 µM of the non-radioactive reference **2f**, 20 µM of CB$_2$R-specific compound GW405833 (Figure 5). As expected upon incubation with [^{18}F]**2f** alone, an important radioactive signal was observed in the spleen. This signal was almost completely inhibited when non-radioactive reference **2f** was co-incubated thus suggesting that compound [^{18}F]**2f** binds in a saturable mechanism as expected for a ligand to receptor interaction. Co-incubation with compound GW405833 displayed almost complete inhibition of the radioactive signal also, proving the specificity of [^{18}F]**2f** for the CB$_2$R.
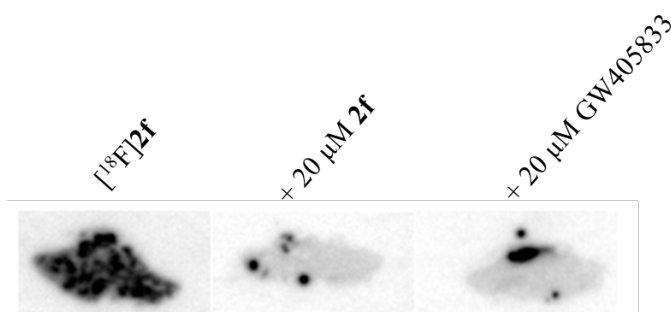
Figure 5. Autoradiographies of a perfused healthy rat (Wistar) spleen incubated with [^{18}F]**2f** alone (111 MBq, 1.0 nmol, 0.56 MBq/mL) or with either 20 μM of the non-radioactive reference **2f** or 20 μM of the CB$_2$R-specific compound GW405833.

Biodistribution and pre-treatment

Biodistribution of [^{18}F]**2f** was evaluated in healthy rats (Wistar) after a bolus i.v. injection of 9-12 MBq (20 MBq/mL, 0.2-0.5 nmol) (Figure 6). A pattern of rapid distribution/elimination of the radioactivity can be observed in all organs except for liver and spleen. In the liver, an accumulation of the radiotracer until 30 min followed by its limited washout at later time points (60 min) indicated a hepato-biliary excretion. This was confirmed by Moldovan *et al.*[26] who observed a hepatic followed by intestine accumulation of radioactivity over 60 min after injection of a fluorine-18-labeled close analog of [^{18}F]**2f**. Such a hepato-biliary excretion was also observed for non-related radiotracers targeting CB$_2$R.[44-47] In the spleen, an important and persistent accumulation of the radioactivity can be observed showing the specific targeting of [^{18}F]**2f** in this CB$_2$R-rich organ. The washout of [^{18}F]**2f** from the spleen could not be observed within the frame of the experiment (60 min) probably due to the high density of CB$_2$R binding sites in the rat spleen, a result already observed by Evens *et al.*.[45]
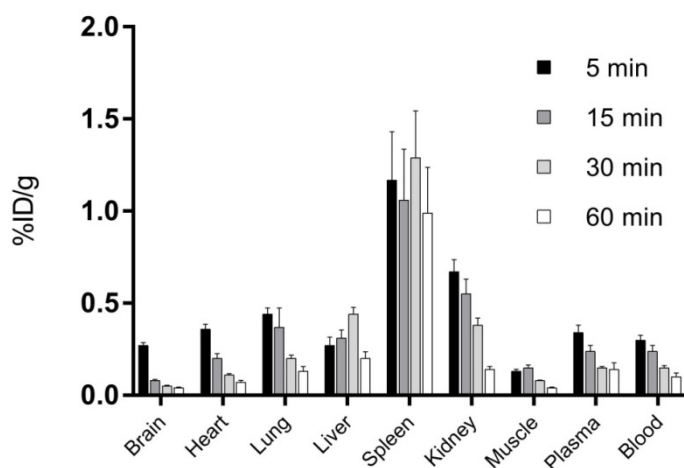
Figure 6. Biodistribution of [^{18}F]**2f** (9-12 MBq, 20 MBq/mL, 0.2-0.5 nmol) in healthy rats (n = 4) over time (5, 15, 30 and 60 min) in different organs. The radioactivity uptake was measured as a percentage of the injected dose per gram of organ (% ID/g)

The specificity of [^{18}F]**2f** for the CB$_2$R was further evaluated in pre-treatment experiments (Figure 7). Three groups of animals (Wistar, n = 3) were pre-treated 15 min before radiotracer injection with either the non-radioactive compound **2f** or GW405833, a selective CB$_2$R agonist or NIDA41020, a selective CB$_1$R antagonist. Control animals were injected with vehicle 15 min before radiotracer injection. Animals were sacrificed 30 min after tracer injection. Pre-treatment with 1.5 mg/kg of **2f** or 1.5 mg/kg of GW405833 showed a strong decrease of the radioactivity uptake in the spleen (P < 0.001) (one-way anova, multiple comparison) whereas pre-treatment with 1.5 mg/kg of NIDA41020 led only to a moderate decrease of the uptake (P > 0.05). This is in agreement with the high physiological expression of CB$_2$R in the spleen and demonstrates the specific binding of [^{18}F]**2f** to the CB$_2$ receptors. In most other organs tested such as the brain or the heart, higher uptake was observed

when animals were pre-treated with either **2f** or GW405833 (Figure S3, see supplementary data) due to a higher plasmatic concentration of the tracer (as observed in Figure S3) resulting from the saturation of the specific sites. No decrease of the signal was observed in the brain when pre-treating with CB_1-specific compound NIDA41020. Assuming that [^{18}F]**2f** enters the brain like [^{18}F]**2c** described by Moldovan *et al.*[26] which is very similar in term of chemical structure, this experiment confirms that our compound does not interact with the CB_1 receptors, thus confirming the selectivity. Moreover, the signal in the brain was very low which was expected considering the weak CB_2R expression in the brain in non-pathological conditions.
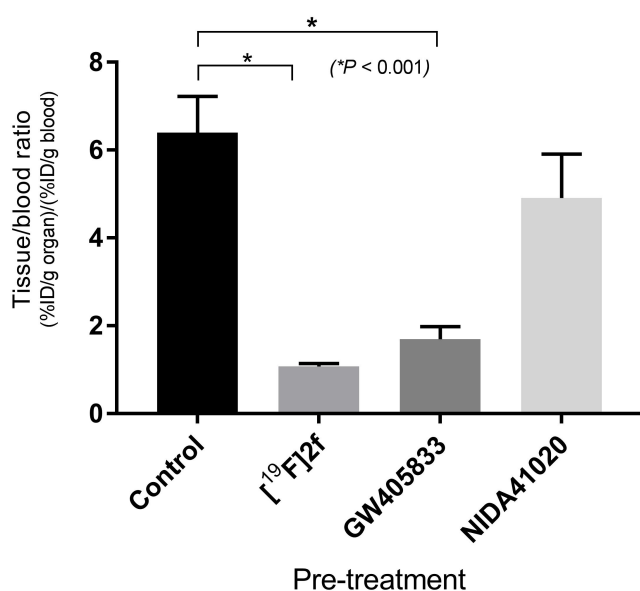
Figure 7. Comparison of the [^{18}F]**2f** uptake in the spleen for control animals and after pre-treatment with either non-radioactive [^{19}F]**2f**, GW405833 or NIDA41020. The values were normalized to %ID/g in blood. The significance (P) was measured using one-way anova.

In vivo metabolism of [^{18}F]2f

Analysis of plasma extracts following *i.v.* administration of [^{18}F]**2f** (42 ± 15 MBq, 20 MBq/mL, 0.38 nmol) to healthy rats was also performed. Radio-HPLC profiles showed three radiometabolite peaks along with [^{18}F]**2f** with retention times at 2 min, 3.5 min, 5.2 min and 7 min respectively (Figure 8A). The main radiometabolite eluted at 2 min was highly polar. Based on the MS/MS experiments and previous studies,[48] this compound may correspond to acidic metabolites, formed by further oxidation of hydroxylated radiometabolites in plasma. These findings are in accordance with the *in vitro* metabolites observed after incubation with rat microsomes (Figure 3D). The percentage of non-metabolized [^{18}F]**2f** exponentially decreased as a function of time representing 53% at 5 min and 25% at 30 min post-injection (Figure 8B). During the same time, the percentage of the main polar radiometabolite increased and reached 50% of plasma radioactivity. The radioactivity measured in the acetonitrile protein precipitates (acetonitrile pellet) increased slowly as a function of time and accounted for only 8% of total plasma radioactivity at 60 min. This radioactivity may be due to the presence of [^{18}F]fluoroacetate (or [^{18}F]fluoroacetic acid) generated by *O*-dealkylation of the tracer. Compared to the recently described analog [^{18}F]**2c** PET radioligand,[26] [^{18}F]**2f** seemed to be more stable as observed in rat plasma (25% at 30 min post injection (p.i.)) than [^{18}F]**2c** in mouse plasma (7% at 30 min p.i.). However, interspecies differences in the *in vivo* metabolism of these compounds may exist.
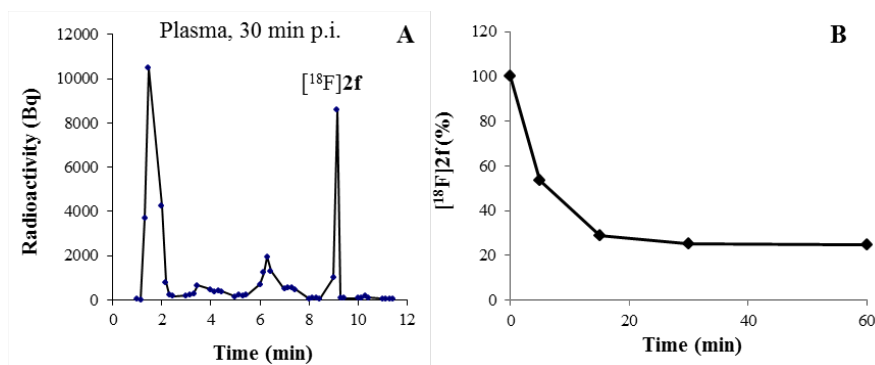
Figure 8. *In vivo* metabolism of [^{18}F]**2f** (42 ± 15 MBq, 20 MBq/mL, 0.38 nmol) in rat plasma (A) Representative radio-HPLC profile and gamma-counting of a 30 min p.i. plasma sample (acetonitrile extraction), (B) Time-course of the percentage of non-metabolized [^{18}F]**2f** in rat plasma.

CONCLUSION

In conclusion, we have developed seven fluorinated analogs of the thiazole derivative A-836339, which all display high affinity for the CB$_2$R and a good selectivity towards the CB$_1$R. All compounds have shown promising ADME properties in terms of lipophilicity, kinetic solubility and membrane permeation capability to target the CB$_2$R *in vivo*. Among them, compound **2f** appeared as the most promising candidate and further investigations revealed good stability in plasma with a free fraction in acceptable range and a favorable metabolic profile showing that compound **2f** meets all the criteria to become an interesting PET tracer for the CB$_2$R. Synthesis of the corresponding tosylated precursor was realized in two steps and radiolabeling with fluorine-18 afforded ready-to-inject [^{18}F]**2f** in good yield and with high molar activity and purity. Biodistribution in healthy rats displayed distribution/elimination patterns for most organs except for the spleen where accumulation was observed, suggesting that [^{18}F]**2f** binds to the CB$_2$R in this CB$_2$R-rich organ. Pre-treatment experiments in rat spleens with either [^{19}F]**2f**, the CB$_2$R-specific compound GW405833 or the CB$_1$-specific compound NIDA41020 confirmed the specificity and the selectivity of **2f** for the CB$_2$R *in vivo*. This promising PET tracer will be further investigated in animal models of inflammation.

References

(1) Aizpurua-Olaizola, O.; Elezgarai, I.; Rico-Barrio, I.; Zarandona, I.; Etxebarria, N.; Usobiaga, A. Targeting the endocannabinoid system: future therapeutic strategies. *Drug Discov Today*, 2017, *22*, 105-110.

(2) Herkenham, M.; Lynn, A.B.; Little, M.D.; Johnson, M.R.; Melvin, L.S.; Decosta, B.R.; Rice, K.C. Cannabinoid receptor localization in brain. *PNAS*, 1990, *87*, 1932-1936.

(3) Klein, T.; Newton, C.; Friedman, H. Cannabinoid receptors and immunity. *Immunol Today*, 1998, *19*, 373-381.

(4) Munro, S.; Thomas, K.L.; Abushaar, M. Molecular characterization of a peripheral receptor for cannabiboids. *Nature*, 1993, *365*, 61-65.

(5) Onaivi, E.S. Neuropsychobiological evidence for the functional presence and expression of cannabinoid CB2 receptors in the brain. *Neuropsychobiol*, 2006, *54*, 231-246.

(6) Van Sickle, M.D.; Duncan, M.; Kingsley, P.J.; Mouihate, A.; Urbani, P.; Mackie, K.; Stella, N.; Makriyannis, A.; Piomelli, D.; Davison, J.S.; Marnett, L.J.; Di Marzo, V.; Pittman, Q.J.; Patel, K.D.; Sharkey, K.A. Identification and functional characterization of brainstem cannabinoid CB2 receptors. *Science*, 2005, *310*, 329-332.

(7) Sheng, W.S.; Hu, S.X.; Min, X.N.; Cabral, G.A.; Lokensgard, J.R.; Peterson, P.K. Synthetic cannabinoid WIN55,212-2 inhibits generation of inflammatory mediators by IL-1b-stimulated human astrocytes. *Glia*, 2005, *49*, 211-219.

(8) Golech, S.A.; McCarron, R.M.; Chen, Y.; Bembry, J.; Lenz, F.; Mechoulam, R.; Shohami, E.; Spatz, M. Human brain endothelium: coexpression and function of vanilloid and endocannabinoid receptors. *Mol Brain Res*, 2004, *132*, 87-92.

(9) Demuth, D.G.; Molleman, A. Cannabinoid signalling. *Life Sci* 2006, *78*, 549-563.

(10) Atwood, B.K.; Wager-Miller, J.; Haskins, C.; Straiker, A.; Mackie, K. Functional selectivity in CB2 cannabinoid receptor signaling and regulation: Implications for the therapeutic potential of CB2 ligands. *Mol Pharmacol*, 2012, *81*, 250-263.

(11) Soethoudt, M.; Grether, U.; Fingerle, J.; Grim, T.W.; Fezza, F.; de Petrocellis, L.; Ullmer, C.; Rothenhausler, B.; Perret, C.; van Gils, N.; Finlay, D.; MacDonald, C.; Chicca, A.; Gens, M.D.; Stuart, J.; de Vries, H.; Mastrangelo, N.; Xia, L.Z.; Alachouzos, G.; Baggelaar, M.P.; Martella, A.; Mock, E.D.; Deng, H.; Heitman, L.H.; Connor, M.; Di Marzo, V.; Gertsch, J.; Lichtman, A.H.; Maccarrone, M.; Pacher, P.; Glass, M.; van der Stelt, M. Cannabinoid CB2 receptor ligand profiling reveals biased signalling and off-target activity. *Nat Comm*, 2017, *8*.

(12) Pisanti, S.; Bifulco, M. Endocannabinoid system modulation in cancer biology and therapy. *Pharm Res* 2009, *60*, 107-116.

(13) Pertwee, R.G. Emerging strategies for exploiting cannabinoid receptor agonists as medicines. *Br J Pharmacol*, 2009, *156*, 397-411.

(14) Aso, E.; Ferrer, I. CB2 cannabinoid receptor as potential target against alzheimer's disease. *Frontiers Neurosc*, 2016, *31*.

(15) Cabral, G.A.; Griffin-Thomas, L. Emerging role of the cannabinoid receptor CB2 in immune regulation: therapeutic prospects for neuroinflammation. *Expert Rev Mol Med*, 2009, *11*.

(16) Price, D.A.; Martinez, A.A.; Seillier, A.; Koek, W.; Acosta, Y.; Fernandez, E.; Strong, R.; Lutz, B.; Marsicano, G.; Roberts, J.L.; Giuffrida, A. WIN55,212-2, a cannabinoid receptor agonist, protects against nigrostriatal cell loss in the 1-methyl-4-phenyl-1,2,3,6-tetrahydropyridine mouse model of Parkinson's disease. *Eur J Neurosci*, 2009, *29*, 2177-2186.

(17) Palazuelos, J.; Aguado, T.; Pazos, M.R.; Julien, B.; Carrasco, C.; Resel, E.; Sagredo, O.; Benito, C.; Romero, J.; Azcoitia, I.; Fernandez-Ruiz, J.; Guzman, M.; Galve-Roperh, I. Microglial CB2 cannabinoid receptors are neuroprotective in Huntington's disease excitotoxicity. *Brain*, 2009, *132*, 3152-3164.

(18) Evens, N.; Bormans, G.M. Non-invasive imaging of the type 2 cannabinoid receptor, focus on Positron Emission Tomography. *Curr Topics Med Chem*, 2010, *10*, 1527-1543.

(19) Vandeputte, C.; Evens, N.; Toelen, J.; Deroose, C.M.; Bosier, B.; Ibrahimi, A.; Van der Perren, A.; Gijsbers, R.; Janssen, P.; Lambert, D.M.; Verbruggen, A.; Debyser, Z.; Bormans, G.; Baekelandt, V.; Van Laere, K. A PET brain reporter gene system based on type 2 cannabinoid receptors. *J Nucl Med*, 2011, *52*, 1102-1109.

(20) Ahmad, R.; Koole, M.; Evens, N.; Serdons, K.; Verbruggen, A.; Bormans, G.; Van Laere, K. Whole-body biodistribution and radiation dosimetry of the cannabinoid type 2 receptor Ligand [¹¹C]NE40 in healthy subjects. *Mol Imaging Biol*, 2013, *15*, 384-390.

(21) Meletta, R.; Slavik, R.; Mu, L.J.; Rancic, Z.; Borel, N.; Schibli, R.; Ametamey, S.M.; Kramer, S.D.; Herde, A.M. Cannabinoid receptor type 2 (CB2) as one of the candidate genes in human carotid plaque imaging: Evaluation of the novel radiotracer [¹¹C]RS-016 targeting CB2 in atherosclerosis. *Nucl Med Biol*, 2017, *47*, 31-43.

(22) Yao, B.B.; Hsieh, G.; Daza, A.V.; Fan, Y.H.; Grayson, G.K.; Garrison, T.R.; El Kouhen, O.; Hooker, B.A.; Pai, M.; Wensink, E.J.; Salyers, A.K.; Chandran, P.; Zhu, C.Z.; Zhong, C.M.; Ryther, K.; Gallagher, M.E.; Chin, C.L.; Tovcimak, A.E.; Hradil, V.P.; Fox, G.B.; Dart, M.J.; Honore, P.; Meyer, M.D. Characterization of a cannabinoid CB2 receptor-selective agonist, A-836339 2,2,3,3-tetramethyl-cyclopropanecarboxylic acid 3-(2-methoxy-ethyl)-4,5-dimethyl-3H-thiazol-(2Z)-ylidene -amide , using *in vitro* pharmacological assays, *in vivo* pain models, and pharmacological magnetic resonance imaging. *J Pharmacol Exp Ther*, 2009, *328*, 141-151.

(23) Horti, A.G.; Gao, Y.J.; Ravert, H.T.; Finley, P.; Valentine, H.; Wong, D.F.; Endres, C.J.; Savonenko, A.V.; Dannals, R.F. Synthesis and biodistribution of [¹¹C]A-836339, a new potential radioligand for PET imaging of cannabinoid type 2 receptors (CB2). *Bioorg Med Chem*, 2010, *18*, 5202-5207.

(24) Savonenko, A.V.; Melnikova, T.; Wang, Y.C.; Ravert, H.; Gao, Y.J.; Koppel, J.; Lee, D.; Pletnikova, O.; Cho, E.; Sayyida, N.; Hiatt, A.; Troncoso, J.; Davies, P.; Dannals, R.F.; Pomper, M.G.; Horti, A.G. Cannabinoid CB2 receptors in a mouse model of Ab amyloidosis: Immunohistochemical analysis and suitability as a PET biomarker of neuroinflammation. *PlosOne*, 2015, *10*.

(25) Pottier, G.; Gomez-Vallejo, V.; Padro, D.; Boisgard, R.; Dolle, F.; Llop, J.; Winkeler, A.; Martin, A. PET imaging of cannabinoid type 2 receptors with [¹¹C]A-836339 did not evidence changes following neuroinflammation in rats. *J Cereb Blood Flow Metab*, 2017, *37*, 1163-1178.

(26) Moldovan, R.P.; Teodoro, R.; Gao, Y.J.; Deuther-Conrad, W.; Kranz, M.; Wang, Y.C.; Kuwabara, H.; Nakano, M.; Valentine, H.; Fischer, S.; Pomper, M.G.; Wong, D.F.; Dannals, R.F.; Brust, P.; Horti, A.G. Development of a high-affinity PET radioligand for imaging cannabinoid subtype 2 receptor. *J Med Chem*, 2016, *59*, 7840-7855.

(27) Zamek-Gliszczynski, M.J.; Ruterbories, K.J.; Ajamie, R.T.; Wickremsinhe, E.R.; Pothuri, L.; Rao, M.V.S.; Basavanakatti, V.N.; Pinjari, J.; Ramanathan, V.K.; Chaudhary, A.K. Validation of 96-well equilibrium dialysis with non-radiolabeled drug for definitive measurement of protein binding and application to clinical development of highly-bound drugs. *J Pharm Sci*, 2011, *100*, 2498-2507.

(28) Miletti, F.; Storchi, L.; Sforna, G.; Cruciani, G. New and original pKa prediction method using grid molecular interaction fields. *J Chem Inf Model*, 2007, *47*, 2172-2181.

(29) Kansy, M.; Senner, F.; Gubernator, K. Physicochemical high throughput screening: Parallel artificial membrane permeation assay in the description of passive absorption processes. *J Med Chem*, 1998, *41*, 1007-1010.

(30) Di, L.; Keefer, C.; Scott, D.O.; Strelevitz, T.J.; Chang, G.; Bi, Y.A.; Lai, Y.R.; Duckworth, J.; Fenner, K.; Troutman, M.D.; Obach, R.S. Mechanistic insights from comparing intrinsic clearance values between human liver microsomes and hepatocytes to guide drug design. *Eur J Med Chem*, 2012, *57*, 441-448.

(31) LeCluyse, E.L.; Witek, R.P.; Andersen, M.E.; Powers, M.J. Organotypic liver culture models: Meeting current challenges in toxicity testing. *Crit Rev Toxicol*, 2012, *42*, 501-548.

(32) Banker, M.J.; Clark, T.H.; Williams, J.A. Development and validation of a 96-well equilibrium dialysis apparatus for measuring plasma protein binding. *J Pharm Sci*, 2003, *92*, 967-974.

(33) Poirier, A.; Cascais, A.C.; Bader, U.; Portmann, R.; Brun, M.E.; Walter, I.; Hillebrecht, A.; Ullah, M.; Funk, C. Calibration of *in vitro* multidrug resistance protein 1 substrate and inhibition assays as a basis to support the prediction of clinically relevant interactions *in vivo*. *Drug Metab Dispos*, 2014, *42*, 1411-1422.

(34) Kremers, P.; Beaune, P.; Cresteil, T.; Degraeve, J.; Columelli, S.; Leroux, J.P.; Gielen, J.E. Cytochrome P-450 mono-oxygenase activities in human and rat-liver microsomes. *Eur J Biochem*, 1981, *118*, 599-606.

(35) Bartholoma, M.D.; Gottumukkala, V.; Zhang, S.H.; Baker, A.; Dunning, P.; Fahey, F.H.; Treves, S.T.; Packard, A.B. Effect of the prosthetic group on the pharmacologic properties of [¹⁸F]labeled

rhodamine B, a potential myocardial perfusion agent for Positron Emission Tomography (PET). *J Med Chem*, 2012, *55*, 11004-11012.

(36) Dollé, F.; Emond, P.; Mavel, S.; Demphel, S.; Hinnen, F.; Mincheva, Z.; Saba, W.; Valette, H.; Chalon, S.; Halldin, C.; Helfenbein, J.; Legaillard, J.; Madelmont, J.C.; Deloye, J.B.; Bottlaender, M.; Guilloteau, D. Synthesis, radiosynthesis and *in vivo* preliminary evaluation of [^{11}C]LBT-999, a selective radioligand for the visualisation of the dopamine transporter with PET. *Bioorg Med Chem*, 2006, *14*, 1115-1125.

(37) Moussa, I.A.; Banister, S.D.; Beinat, C.; Giboureau, N.; Reynolds, A.J.; Kassiou, M. Design, synthesis, and structure-affinity relationships of regioisomeric *N*-benzyl alkyl ether piperazine derivatives as sigma-1 receptor ligands. *J Med Chem*, 2010, *53*, 6228-6239.

(38) Perera, S.; Piwnica-Worms, D.; Alauddin, M.M. Synthesis of a F-18 -labeled ceritinib analogue for positron emission tomography of anaplastic lymphoma kinase, a receptor tyrosine kinase, in lung cancer. *J Label Compds Radiopharm*, 2016, *59*, 103-108.

(39) Ullmer, C.; Zoffmann, S.; Bohrmann, B.; Matile, H.; Lindemann, L.; Flor, P.J.; Malherbe, P. Functional monoclonal antibody acts as a biased agonist by inducing internalization of metabotropic glutamate receptor 7. *Br J Pharmacol*, 2012, *167*, 1448-1466.

(40) Honer, M.; Gobbi, L.; Martarello, L.; Comley, R.A. Radiologand development for molecular imaging of the central nervous system with positron emission tomography. *Drug Discov Today*, 2014, *19*, 1936-1944.

(41) Ryckmans, T.; Edwards, M.P.; Horne, V.A.; Correia, A.M.; Owen, D.R.; Thompson, L.R.; Tran, I.; Tutt, M.F.; Young, T. Rapid assessment of a novel series of selective CB2 agonists using parallel synthesis protocols: A Lipophilic Efficiency (LipE) analysis. *Bioorg Med Chem Lett*, 2009, *19*, 4406-4409.

(42) Tecle, B.; Casida, J.E. Enzymatic defluorination and metabolism of fluoroacetate, fluoroacetamide, fluoroethanol, and (-)erythro-fluorocitrate in rats and mice examined bi ^{19}F-NMR and ^{13}C-NMR. *Chem Res Toxical*, 1989, *2*, 429-435.

(43) Kuchar, M.; Mamat, C. Methods to increase the metabolic stability of ^{18}F-radiotracers. *Molecules*, 2015, *20*, 16186-16220.

(44) Evens, N.; Muccioli, G.G.; Houbrechts, N.; Lambert, D.M.; Verbruggen, A.M.; Van Laere, K.; Bormans, G.M. Synthesis and biological evaluation of carbon-11-and fluorine-18-labeled 2-oxoquinoline derivatives for type 2 cannabinoid receptor positron emission tomography imaging. *Nucl Med Biol*, 2009, *36*, 455-465.

(45) Evens, N.; Vandeputte, C.; Coolen, C.; Janssen, P.; Sciot, R.; Baekelandt, V.; Verbruggen, A.M.; Debyser, Z.; Van Laere, K.; Bormans, G.M. Preclinical evaluation of [^{11}C]NE40, a type 2 cannabinoid receptor PET tracer. *Nucl Med Biol*, 2012, *39*, 389-399.

(46) Evens, N.; Vandeputte, C.; Muccioli, G.G.; Lambert, D.M.; Baekelandt, V.; Verbruggen, A.M.; Debyser, Z.; Van Laere, K.; Bormans, G.M. Synthesis, *in vitro* and *in vivo* evaluation of fluorine-18 labelled FE-GW405833 as a PET tracer for type 2 cannabinoid receptor imaging. *Bioorg Med Chem*, 2011, *19*, 4499-4505.

(47) Haider, A.; Herde, A.M.; Slavik, R.; Weber, M.; Mugnaini, C.; Ligresti, A.; Schibli, R.; Mu, L.J.; Ametamey, S.M. Synthesis and biological evaluation of thiophene-based cannabinoid receptor type 2 radiotracers for PET imaging. *Frontiers Neurosci*, 2016, *10*.

(48) Peyronneau, M.A.; Saba, W.; Goutal, S.; Damont, A.; Dolle, F.; Kassiou, M.; Bottlaender, M.; Valette, H. Metabolism and quantification of [^{18}F]DPA-714, a New TSPO positron emission tomography radioligand. *Drug Metab Dispos*, 2013, *41*, 122-131.

For Table of Contents use only

From Structure-Activity Relationships on Thiazole Derivatives to the *In Vivo* Evaluation of a New Radiotracer for Cannabinoid Subtype 2 PET Imaging

Fabien Caillé[†,1] Fanny Cacheux[†,1] Marie-Anne Peyronneau,[1] Benoît Jego,[1] Emilie Jaumain,[1] Géraldine Pottier,[1] Christoph Ullmer,[2] Uwe Grether,[2] Alexandra Winkeler,[1] Frédéric Dollé,[1] Annelaure Damont[1] and Bertrand Kuhnast[*,1]
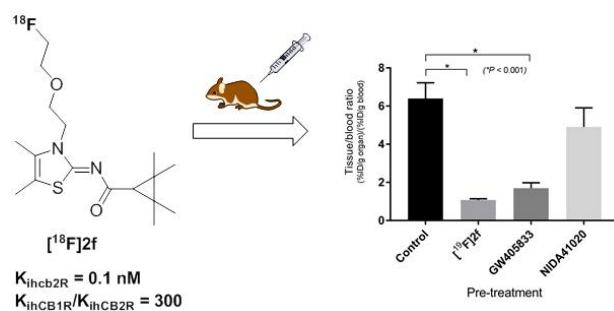
Supporting information for:

From Structure-Activity Relationships on Thiazole Derivatives to the *In Vivo* Evaluation of a New Radiotracer for Cannabinoid Subtype 2 PET Imaging

Fabien Caillé[†,1] Fanny Cacheux[†,1] Marie-Anne Peyronneau,[1] Emilie Jaumain,[1] Benoît Jego,[1] Géraldine Pottier,[1] Christoph Ullmer,[2] Uwe Grether,[2] Alexandra Winkeler,[1] Frédéric Dollé,[1] Annelaure Damont[1] and Bertrand Kuhnast[*,1]

[1]UMR 1023 IMIV, Service Hospitalier Frédéric Joliot, CEA, Inserm, Université Paris Sud, CNRS, Université Paris-Saclay, Orsay, France
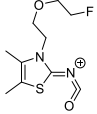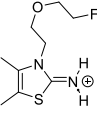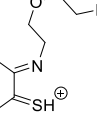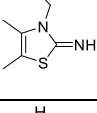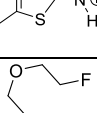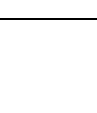
[2]Roche Innovation Center Basel, F. Hoffmann-La Roche Ltd., Basel, Switzerland

[*]corresponding author: bertrand.kuhnast@cea.fr

ORCID iD Bertrand Kuhnast : 0000-0002-5035-4072

[†] these authors contributed equally to this work

Table S1. Positive ion ESI-MS [M+H$^+$] and predominant MS^2 and MS^3 fragments obtained for **2f** and its main metabolites.

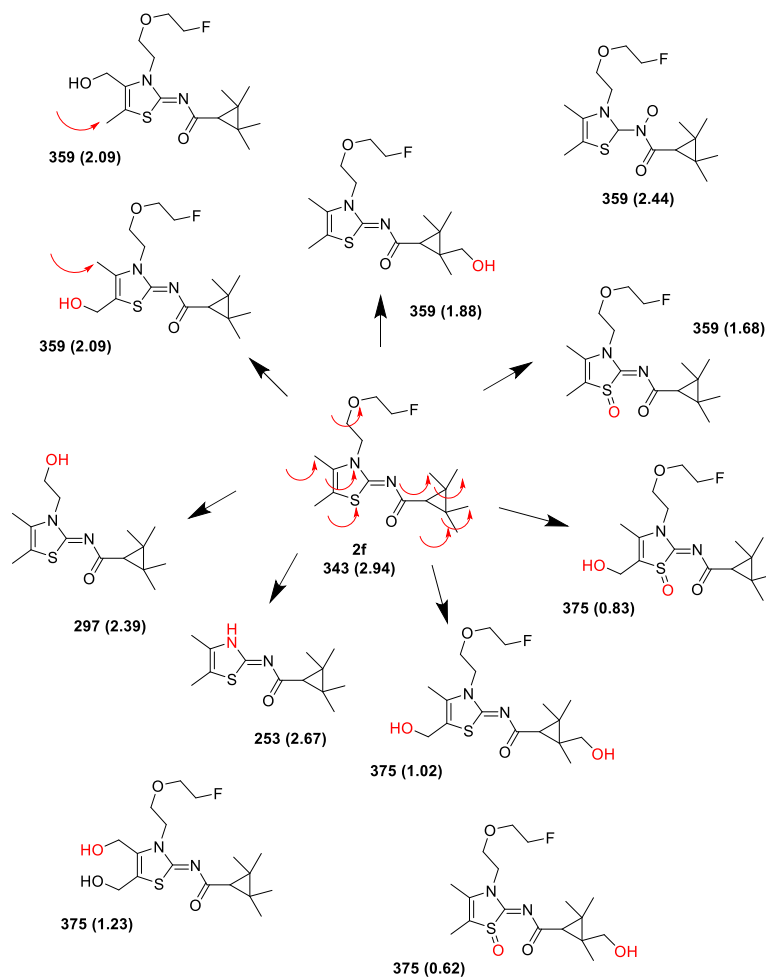| Compound	2f	M1	M2	M3	M4	M5	M6
[M+H+]	**343**	**359**	**359**	**375**	**297**	**359**	**375**
RT	6.41	5.78	5.48	5.28	5.29	4.55	3.90
(structure)	**245**			261		245	261
(structure)	**219**	235	235	235	173	219	251
(structure)	**192**		208				
(structure)	**155**	171	171		156	155	155
(structure)	**129**	127	146		130		
(structure)	**91**	91	91			91	91

Figure S1. Proposed metabolic pathways for **2f** with potential sites of oxidation (red arrows). The numbers between brackets represent the lipophilicity (logP).
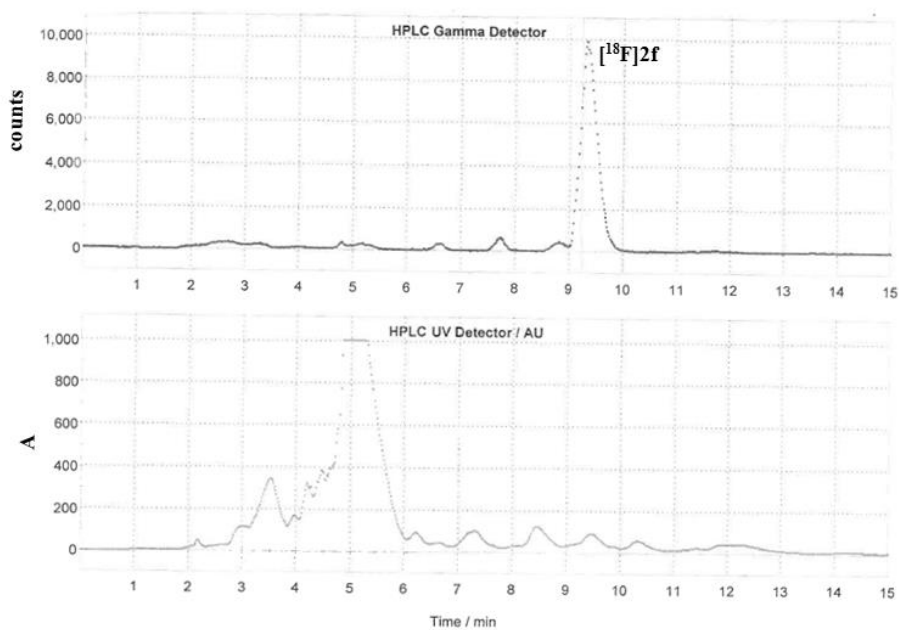
Figure S2. Semi-preparative HPLC with gamma detection (top) and UV detection (bottom) for purification of [^{18}F]**2f**.
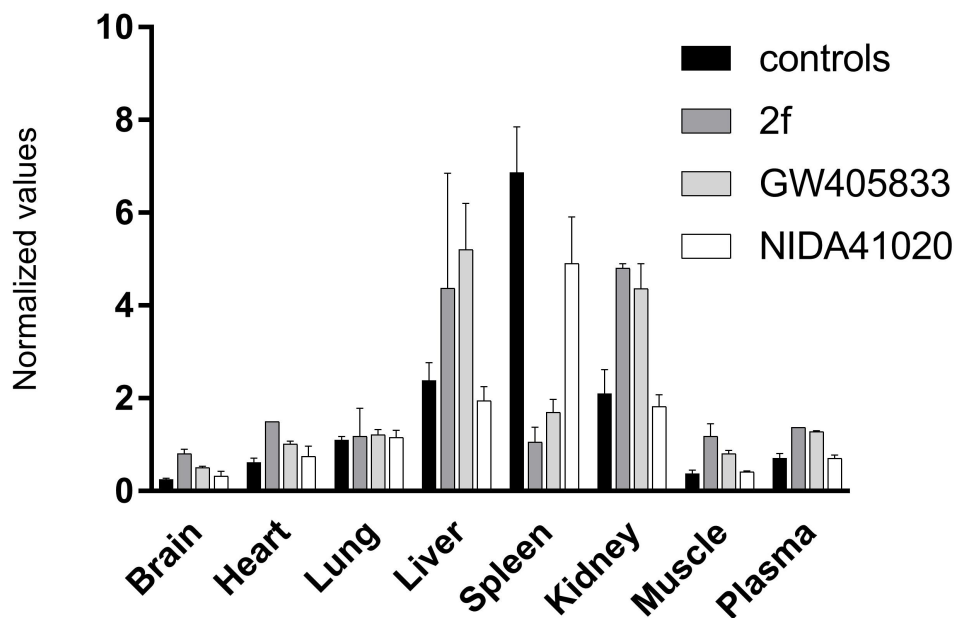

Figure S3. Biodistribution of [^{18}F]**2f** on healthy rats with or without presaturation.